

Euler top with a rotor: classical analogies of spin squeezing and quantum phase transitions in a generalized Lipkin-Meshkov-Glick model

Tomáš Opatrný, Lukáš Richterek, and Martin Opatrný

Palacký University, Faculty of Science, 17. Listopadu 12, 77146 Olomouc, Czech Republic

(Dated: August 28, 2017)

We show that the classical model of Euler top (freely rotating, generally asymmetric rigid body), possibly supplemented with a rotor, corresponds to a generalized Lipkin-Meshkov-Glick (LMG) model describing phenomena of various branches of quantum physics. Classical effects such as free precession of a symmetric top, Feynman's wobbling plate, tennis-racket instability and the Dzhanibekov effect, attitude control of satellites by momentum wheels, or twisting somersault dynamics, have their counterparts in quantum effects that include spin squeezing by one-axis twisting and two-axis countertwisting, transitions between the Josephson and Rabi regimes of a Bose-Einstein condensate in a double-well potential, and other quantum critical phenomena. The parallels enable us to expand the range of explored quantum phase transitions in the generalized LMG model, as well as to present a classical analogy of the recently proposed LMG Floquet time crystal.

I. INTRODUCTION

“*The same equations have the same solutions*” is a well known Feynman's quote from his lecture on electrostatic analogs [1]. Taking advantage of known solutions of Maxwell's equations, Feynman shows how to apply them for solving problems of heat transport, neutron diffusion, fluid dynamics, and photometry. The message is that analogs are powerful tools that allow the exchange of know-how between different branches of physics. Here we follow this approach and focus on quantum analogs of the Euler dynamical equations, initially introduced to study rotations of rigid bodies [2]. We show that already the simplest version of Euler equations describing a free spinning top is relevant to the quantum mechanical problem of spin squeezing [3, 4], i.e., noise suppression important for improving precision of atomic clocks and measuring devices. If a freely spinning rotor with its axis fixed with respect to the top is added, plethora of new phenomena occur with analogies across diverse fields. Equations of motion that were originally purely quadratic get additional linear terms. As a consequence, one can observe features of the Lipkin-Meshkov-Glick (LMG) model of nuclear physics [5], excited state quantum phase transitions [6–8], self-trapping of Bose-Einstein condensates in potential wells [9, 10], or twist-and-turn scenario of spin squeezing [11]. These quantum phenomena correspond to purely classical effects such as satellite stabilization by momentum wheels [12–14] or motion of an athlete executing a twisted somersault [15, 16].

The aim of this paper is to identify mutually equivalent relations of various fields and help the reader to use the intuition accumulated in one branch of physics for solving problems of another. We apply here this approach to show new types of excited state quantum phase transitions in a generalized LMG model that correspond to different kinds of motion in rigid body dynamics. We also propose a classical analogue of the recently introduced LMG Floquet time crystal [17].

The paper is organized in such a way that more com-

plex models follow the simple ones. In Sec. II the basic equations are introduced. In Sec. III analogies between motion of a symmetric top and spin squeezing by one-axis twisting are studied. In Sec. IV we deal with the asymmetric top, tennis-racket instability, and two-axis countertwisting scenario of spin squeezing. In Sec. V the dynamics of a symmetric top with a coaxial rotor and their quantum analogies are studied. Sec. VI is focused on a symmetric top with a perpendicular rotor and the corresponding quantum model with effects such as the twist-and-turn spin squeezing scenario, or transitions between the Rabi and Josephson regimes in trapped Bose-Einstein condensates. Sec. VII deals with the main features of an asymmetric top with a rotor along one of the principal axes and their analogies in the LMG model. In Sec. VIII we present a general treatment of stationary angular momenta and their stability, relevant to the excited-state quantum phase transitions in a generalized LMG model. In Sec. IX we introduce a classical analogue of the LMG time crystal, and we conclude with Sec. X. Some lengthy formulas and derivations are presented in Appendixes.

II. EQUATIONS OF MOTION

A. Classical motion

Evolution of the angular momentum \vec{L} of a rigid body is governed by the equation

$$\frac{d\vec{L}}{dt} = \vec{M}, \quad (1)$$

where \vec{M} is the torque. We use the relation between the time derivative $d\vec{A}/dt$ of a vector \vec{A} in an inertial coordinate system and the time derivative $d'\vec{A}/dt$ in a coordinate system that rotates with angular velocity $\vec{\omega}$ with respect to the inertial system

$$\frac{d'\vec{A}}{dt} = \frac{d\vec{A}}{dt} - \vec{\omega} \times \vec{A}. \quad (2)$$

Applying that on Eq. (1), we get

$$\frac{d'\vec{L}}{dt} = \vec{M} - \vec{\omega} \times \vec{L}. \quad (3)$$

Assume that the torque stems from a rotor whose axis is fixed with respect to the rigid body as in Fig. 1. We have

$$\vec{M} = -\vec{M}_{\text{rotor}} = -\frac{d\vec{K}}{dt}, \quad (4)$$

where \vec{M}_{rotor} is the torque with which the rigid body acts on the rotor with angular momentum \vec{K} . Using the expression for the time derivative in the rotating system, we have

$$\begin{aligned} \vec{M} &= -\frac{d'\vec{K}}{dt} - \vec{\omega} \times \vec{K} \\ &= -\vec{\omega} \times \vec{K}, \end{aligned} \quad (5)$$

since $d'\vec{K}/dt = 0$ as the rotor changes neither the magnitude of rotation nor the axis orientation with respect to the rigid body. Using this in Eq. (3) we have

$$\frac{d'\vec{L}}{dt} = -\vec{\omega} \times (\vec{L} + \vec{K}). \quad (6)$$

If the axes of the rotating coordinate system are the principal axes of the tensor of inertia of the body, we have

$$L_k = I_k \omega_k, \quad k = 1, 2, 3, \quad (7)$$

where $I_{1,2,3}$ are the principal moments of inertia. This allows us to write

$$\begin{aligned} \dot{\omega}_1 &= \frac{I_2 - I_3}{I_1} \omega_2 \omega_3 + \frac{K_2 \omega_3 - K_3 \omega_2}{I_1}, \\ \dot{\omega}_2 &= \frac{I_3 - I_1}{I_2} \omega_3 \omega_1 + \frac{K_3 \omega_1 - K_1 \omega_3}{I_2}, \\ \dot{\omega}_3 &= \frac{I_1 - I_2}{I_3} \omega_1 \omega_2 + \frac{K_1 \omega_2 - K_2 \omega_1}{I_3}, \end{aligned} \quad (8)$$

where the dot denotes time derivative in the rotating system. These are the well known Euler dynamical equations which for $\vec{K} = 0$ correspond to a free top, and here the special case corresponds to the torque coming from the rotor. These equations can be expressed in terms of the angular momentum,

$$\begin{aligned} \dot{L}_1 &= \left(\frac{1}{I_3} - \frac{1}{I_2}\right) L_2 L_3 + \frac{K_2}{I_3} L_3 - \frac{K_3}{I_2} L_2, \\ \dot{L}_2 &= \left(\frac{1}{I_1} - \frac{1}{I_3}\right) L_3 L_1 + \frac{K_3}{I_1} L_1 - \frac{K_1}{I_3} L_3, \\ \dot{L}_3 &= \left(\frac{1}{I_2} - \frac{1}{I_1}\right) L_1 L_2 + \frac{K_1}{I_2} L_2 - \frac{K_2}{I_1} L_1. \end{aligned} \quad (9)$$

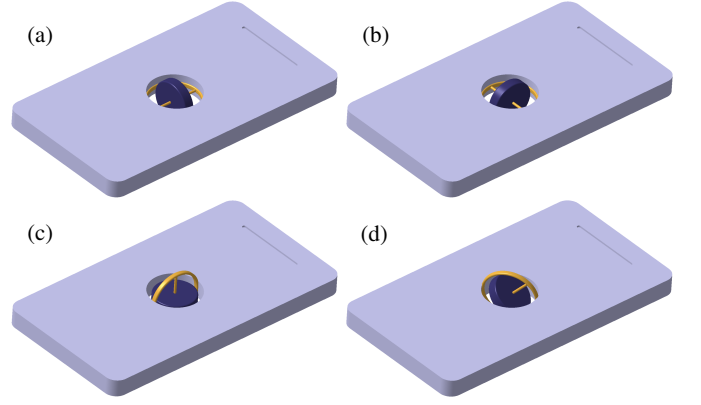


FIG. 1: Rigid bodies supplemented with a rotor. In panels (a)–(c) the rotor axis lies along one of the principal axes of the body, in panel (d) the rotor axis has general orientation.

It is suitable to work with the total angular momentum $\vec{J} \equiv \vec{L} + \vec{K}$, for which one finds

$$\begin{aligned} \dot{J}_1 &= \left(\frac{1}{I_3} - \frac{1}{I_2}\right) J_2 J_3 + \frac{K_2}{I_2} J_3 - \frac{K_3}{I_3} J_2, \\ \dot{J}_2 &= \left(\frac{1}{I_1} - \frac{1}{I_3}\right) J_3 J_1 + \frac{K_3}{I_3} J_1 - \frac{K_1}{I_1} J_3, \\ \dot{J}_3 &= \left(\frac{1}{I_2} - \frac{1}{I_1}\right) J_1 J_2 + \frac{K_1}{I_1} J_2 - \frac{K_2}{I_2} J_1. \end{aligned} \quad (10)$$

As can be checked, the evolution equations conserve the kinetic energy of the rigid body and the magnitude of the total angular momentum, i.e.,

$$\dot{E}_{\text{body}} = 0, \quad \dot{J}^2 = 0, \quad (11)$$

where

$$E_{\text{body}} = \frac{L_1^2}{2I_1} + \frac{L_2^2}{2I_2} + \frac{L_3^2}{2I_3}, \quad (12)$$

$$J^2 = J_1^2 + J_2^2 + J_3^2. \quad (13)$$

Thus, the trajectories in the angular momentum space are intersections of the energy ellipsoid $E_{\text{body}} = \text{const}$ and the total angular momentum sphere $J = \text{const}$, their centers being displaced by \vec{K} . This geometric interpretation is especially helpful for finding stationary angular momenta and determining their stability.

B. Quantum motion

Assume two bosonic modes described by annihilation operators \hat{a} and \hat{b} with total number of particles N . These operators commute as $[\hat{a}, \hat{a}^\dagger] = [\hat{b}, \hat{b}^\dagger] = 1$ and the remaining commutators vanish. One can introduce

operator $\hat{\vec{J}}$ with components defined as

$$\hat{J}_x = \frac{1}{2}(\hat{a}^\dagger \hat{b} + \hat{a} \hat{b}^\dagger), \quad (14)$$

$$\hat{J}_y = \frac{1}{2i}(\hat{a}^\dagger \hat{b} - \hat{a} \hat{b}^\dagger), \quad (15)$$

$$\hat{J}_z = \frac{1}{2}(\hat{a}^\dagger \hat{a} - \hat{b}^\dagger \hat{b}), \quad (16)$$

with $N = \hat{a}^\dagger \hat{a} + \hat{b}^\dagger \hat{b}$. These operators satisfy the angular momentum commutation relations $[\hat{J}_x, \hat{J}_y] = i\hat{J}_z$, $[\hat{J}_y, \hat{J}_z] = i\hat{J}_x$, and $[\hat{J}_z, \hat{J}_x] = i\hat{J}_y$. Assume a general quadratic Hamiltonian in the form

$$\hat{H} = \sum_{k,l} \chi_{kl} \hat{J}_k \hat{J}_l + \sum_k \Omega_k \hat{J}_k, \quad (17)$$

where the indexes k, l run through x, y, z , the quantities $\chi_{kl} = \chi_{lk}$ are components of a twisting tensor χ [18], and we put $\hbar = 1$. As discussed below, this Hamiltonian describes dynamics of symmetrical samples of interacting two-level systems in the Lipkin-Meshkov-Glick model [5], as well as various regimes of spin squeezing [3].

By a suitable rotation of the coordinate system, the twisting tensor can be cast into diagonal form such that the Hamiltonian is

$$\hat{H} = \sum_{k=1}^3 \left(\chi_k \hat{J}_k^2 + \Omega_k \hat{J}_k \right), \quad (18)$$

where χ_k are the eigenvalues of the twisting tensor and the commutation rules are $[\hat{J}_1, \hat{J}_2] = i\hat{J}_3$ with cyclic permutations. The Heisenberg evolution equations $i d\hat{A}/dt = [\hat{A}, \hat{H}]$ then yield

$$\begin{aligned} \frac{d\hat{J}_1}{dt} &= (\chi_2 - \chi_3)(\hat{J}_2 \hat{J}_3 + \hat{J}_3 \hat{J}_2) + \Omega_2 \hat{J}_3 - \Omega_3 \hat{J}_2, \\ \frac{d\hat{J}_2}{dt} &= (\chi_3 - \chi_1)(\hat{J}_3 \hat{J}_1 + \hat{J}_1 \hat{J}_3) + \Omega_3 \hat{J}_1 - \Omega_1 \hat{J}_3, \\ \frac{d\hat{J}_3}{dt} &= (\chi_1 - \chi_2)(\hat{J}_1 \hat{J}_2 + \hat{J}_2 \hat{J}_1) + \Omega_1 \hat{J}_2 - \Omega_2 \hat{J}_1. \end{aligned} \quad (19)$$

Note that Hamiltonian (18) commutes with the total angular momentum so that \hat{J}^2 is a conserved quantity with $\hat{J}^2 \equiv \hat{J}_1^2 + \hat{J}_2^2 + \hat{J}_3^2 = \frac{N}{2}(\frac{N}{2} + 1)$.

C. Correspondence of the models

Equations (19) and (10) have the same structure, except for (10) being classical equations whereas (19) are operator equations with symmetrized products of operators. Thus, both models yield analogous predictions. This happens for short times provided the quantum system was initialized in a classical-like spin coherent state. For longer times, interference phenomena occur and the predictions of the two models deviate.

The two sets of equations correspond to each other provided we make the change

$$\chi_k \leftrightarrow -\frac{1}{2I_k}, \quad \Omega_k \leftrightarrow \frac{K_k}{I_k}, \quad (20)$$

or

$$I_k \leftrightarrow -\frac{1}{2\chi_k}, \quad K_k \leftrightarrow -\frac{\Omega_k}{2\chi_k}. \quad (21)$$

Note that the dimension of the quantities is set by our choice $\hbar = 1$; to have the usual dimensionality, the relation between χ_k and I_k would be changed to $\chi_k \leftrightarrow -\hbar/(2I_k)$.

Note also that, whereas there is a straightforward correspondence between the quantum and classical angular momenta $\hat{\vec{J}} \leftrightarrow \vec{J}$, the relation between the energy of the body (12) and the quantum Hamiltonian (18) is rather

$$\hat{H} \leftrightarrow -E_{\text{body}} + \sum_{k=1}^3 \frac{K_k^2}{2I_k}. \quad (22)$$

The last term is a constant that can be considered trivial. On the other hand, the difference of signs of \hat{H} and E_{body} is interesting: as a result, the quantum vector $\hat{\vec{J}}$ moves on the sphere of $\hat{J}^2 = \text{const}$ along a constant energy contour such that the higher energy area is on the left, the classical vector \vec{J} moves on the sphere of $J^2 = \text{const}$ with the higher energy area on the right.

D. Invariance with respect to transformation of χ_k and I_k

Since in Eq. (19) only the differences between the twisting tensor eigenvalues occur, the dynamics are not changed if a constant is added to all eigenvalues of χ , i.e., $\chi_k \rightarrow \chi_k + \chi_0$. This transformation just shifts the Hamiltonian by a constant $\chi_0 \hat{J}^2$. This means one has a freedom in choosing a reference value of χ . The same holds in the classical dynamics if the moments of inertia are modified as

$$\frac{1}{I_k} \rightarrow \frac{1}{I_k} + \frac{1}{I_0} \quad (23)$$

and the angular momentum of the rotor as

$$K_k \rightarrow \frac{K_k}{1 + \frac{I_k}{I_0}} \quad (24)$$

with I_0 independent of k . With J fixed, the energy of the body is then shifted by

$$\Delta E_{\text{body}} = \frac{J^2}{2I_0} - \sum_{k=1}^3 \frac{K_k^2}{2(I_0 + I_k)}. \quad (25)$$

As a consequence, for any quantum system described by twisting tensor χ and frequency vector $\vec{\Omega}$, one can find

a classical rigid body characterized by tensor of inertia I supplemented with a rotor with angular momentum \vec{K} such that the combined system has the same dynamics. To show that, recall that mass can be assembled such as to have arbitrary principal moments of inertia I_k , provided these values are positive and satisfy the triangle inequality $I_j \leq I_k + I_l$ for any permutation of indexes j, k, l . The first condition is satisfied by a suitable choice of the additive constant χ_0 making all values χ_k negative such that all values I_k resulting from Eq. (21) are positive. If the resulting values I_k violate the triangle inequality, one can fix it as follows. Assume that, say, $I_1 > I_2 + I_3$. Then, by choosing I_0 satisfying

$$0 < I_0 < \frac{I_2 I_3 + \sqrt{I_2^2 I_3^2 + I_1 I_2 I_3 (I_1 - I_2 - I_3)}}{I_1 - I_2 - I_3} \quad (26)$$

and applying Eq. (23), one finds a realistic tensor of inertia corresponding to the given twisting tensor χ . The linear part of the equations of motion can then easily be adjusted by a suitable choice of \vec{K} .

Let us note that the invariance with respect to transformations (23) is valid only for the dynamics of momenta, Eqs. (9) or (10), but not for the evolution of the angular velocity, Eq. (8). This means that one can mutually map the quantum and classical evolution only with respect to where the angular momentum points, but not with respect to how the rigid body is oriented itself. The latter would follow from the kinematic Euler equations which are not included in our study. We anticipate that with expanding the analogy, the classical body orientation would be related to the global phase of the quantum system. Even though connections to other interesting phenomena might be found, such as, e.g., the Montgomery phase [19, 20] referring to the change of body orientation after \vec{J} returns to its initial value, these are beyond the scope of this paper.

E. Lipkin-Meshkov-Glick model

In 1965 Lipkin, Meshkov and Glick formulated a toy model of multiparticle interaction that can be, under certain conditions, solved exactly, and thus serve as a basis for testing various approximation methods [5]. Although the original motivation was in modeling energy spectra of atomic nuclei, the scheme turned out to be useful for studying interesting phenomena in more general systems. These include quantum criticality and phase transitions [21–31], multi-particle entanglement [21, 32–35], spin squeezing [3, 4, 10, 11, 18, 36–70], molecular magnetism [71], or circuit quantum electrodynamics [72].

The LMG Hamiltonian can be written in the form

$$\hat{H} = \epsilon \hat{J}_3 + V(\hat{J}_1^2 - \hat{J}_2^2) + W(\hat{J}_1^2 + \hat{J}_2^2), \quad (27)$$

where ϵ, V and W are real parameters. In the original paper [5] the LMG model describes N fermions in two degenerate levels whose energies differ by ϵ . The term

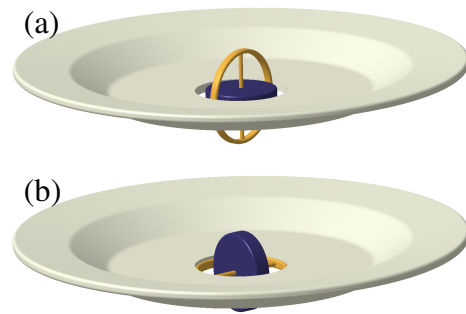


FIG. 2: Plate as a symmetric top with a coaxial rotor (a), and with a perpendicular axis rotor (b).

proportional to V scatters pairs of particles of the same level to the other level, and the term proportional to W scatters one particle up while another particle is scattered down.

As discussed in Sec. II B, the quadratic part of the Hamiltonian corresponds to the diagonal twisting tensor χ ,

$$\chi = \begin{pmatrix} W + V & 0 & 0 \\ 0 & W - V & 0 \\ 0 & 0 & 0 \end{pmatrix}. \quad (28)$$

Since any multiple of a unit tensor can be added to χ without changing the dynamics, any diagonal χ can be expressed in a form equivalent to (28). In particular, for a diagonal χ with terms χ_1, χ_2, χ_3 , by subtracting χ_3 from all the diagonal terms, one gets the LMG parameters $W = (\chi_1 + \chi_2)/2 - \chi_3$ and $V = (\chi_1 - \chi_2)/2$. Since for general quadratic Hamiltonians the labeling of principal axes 1,2,3 is arbitrary, any quadratic Hamiltonian with the linear part parallel to one of the principal axes is equivalent to the LMG Hamiltonian (27). Thus, in the classical analogy, the LMG model corresponds to a freely rotating rigid body supplemented with a rotor with its rotational axis fixed along one of the principal axes of the body as in Fig. 1 (a)–(c). The special case of $V = 0$ corresponds to a symmetrical top with an coaxial rotor as, e.g., in Fig. 2(a). For $W > 0$ the top is a prolate and for $W < 0$ oblate. For $V = W$ the LMG model corresponds to a symmetric top with a perpendicular axis rotor as, e.g., in Fig. 2(b), with $W > 0$ referring to oblate and $W < 0$ to prolate tops.

III. FREE SYMMETRIC TOP, FEYNMAN'S PLATE, AND SPIN SQUEEZING BY ONE-AXIS TWISTING

As the simplest model, consider a symmetric top with $I_1 = I_2 \neq I_3$ with no rotor, i.e., $K_k = 0$. Equations (8)

then simplify to

$$\begin{aligned}\dot{\omega}_1 &= -\tilde{\Omega}\omega_2, \\ \dot{\omega}_2 &= \tilde{\Omega}\omega_1, \\ \dot{\omega}_3 &= 0,\end{aligned}\quad (29)$$

where

$$\tilde{\Omega} \equiv \frac{I_3 - I_1}{I_1}\omega_3 = \left(\frac{1}{I_1} - \frac{1}{I_3}\right)J_3. \quad (30)$$

In quantum domain this corresponds to Hamiltonian (18) reduced to

$$\hat{H}_{\text{OAT}} = \chi \hat{J}_3^2 \quad (31)$$

with

$$\chi = \frac{1}{2I_1} - \frac{1}{2I_3}. \quad (32)$$

The subscript ‘‘OAT’’ in Eq. (31) refers to the ‘‘one-axis twisting’’ scenario of spin squeezing described below.

A. Classical dynamics

Textbooks show solutions of Eq. (29) as regular precession of the top [73, 74],

$$\begin{aligned}\omega_1 &= A \cos \tilde{\Omega}t, \\ \omega_2 &= A \sin \tilde{\Omega}t,\end{aligned}\quad (33)$$

where the amplitude is $A = \sqrt{\omega_1^2 + \omega_2^2} = \sqrt{\omega^2 - \omega_3^2}$. Thus, in the frame fixed with the body, the axis of rotation circles with frequency $\tilde{\Omega}$ around the symmetry axis of the top. For $A \ll \omega_3$, i.e., for small angles between the rotation axis and the symmetry axis, an external observer sees the top wobbling with frequency $\omega_3 + \tilde{\Omega}$. Two extreme cases of the mass distribution in the top correspond to a flat, plate-like top with $I_3 \rightarrow 2I_1$, and a rod-like top with $I_3 \rightarrow 0$. The plate-like top has $\tilde{\Omega} \rightarrow \omega_3$ so that the wobbling frequency is $\approx 2\omega_3$, and the rod-like top has $\tilde{\Omega} \rightarrow -\omega_3$ so that the wobbling frequency tends to zero (one can see that when throwing up a spinning pencil).

Feynman in his book ‘‘Surely, You Are Joking, Mr. Feynman!’’ [75] tells a story: ‘‘. . . I was in the [Cornell] cafeteria and some guy, fooling around, throws a plate in the air. As the plate went up in the air I saw it wobble, and I noticed the red medallion of Cornell on the plate going around. It was pretty obvious to me that the medallion went around faster than the wobbling. I had nothing to do, so I start to figure out the motion of the rotating plate. I discover that when the angle is very slight, the medallion rotates twice as fast as the wobble rate—two to one. It came out of a complicated equation!’’ Feynman was surely joking when telling this story to R. Leighton who collected Feynman’s memories, because the situation is just opposite: the wobbling is twice as fast as the

rotation. This follows from the above arguments, and was clearly explained in a note by B. F. Chao [76] four years after Feynman’s book, as well as in a more detailed study in [77].

Consider now the situation when the top is spun around an axis lying in the symmetry plane, as with coin tossing (see, e.g., [78]). If $\omega_3 = 0$, then $\tilde{\Omega} = 0$ and the rotational axis keeps its orientation. If the rotational axis is oriented slightly off the symmetry plane, it slowly precesses with a speed proportional to its deviation of the plane. For oblate tops ($I_1 < I_3$) the projection of the precession velocity to the symmetry axis has the same orientation as the projection of the rotational axis, $\tilde{\Omega}/\omega_3 > 0$; for prolate tops ($I_1 > I_3$) the situation is opposite, $\tilde{\Omega}/\omega_3 < 0$.

B. Quantum dynamics and spin squeezing

The one-axis twisting (OAT) scenario of spin squeezing corresponding to Hamiltonian (31) was first proposed theoretically by Kitagawa and Ueda [3]. Based on proposals specifying various mechanisms (e.g., [4, 36, 39, 41, 46]) it was observed experimentally in hyperfine states of individual atoms [42, 43], in collective spins of atomic samples interacting by spin-dependent collisions [37, 44, 47, 48], and by optically mediated dispersive interaction in near-resonant cavities [49]. Other proposals for OAT realization include nuclear spins in quantum dots [51, 64], phonon-induced interactions of spins in diamond nanostructures [53], or cold paramagnetic molecules [61].

For an intuitive picture of OAT spin squeezing, consider N two-level atoms initially prepared in the same spin state: as a whole, the system is in spin coherent state. Collective spin states can be visualized on the Bloch sphere with coordinates $J_{1,2,3}$ as in Fig. 3(a). The initial spin coherent state is represented by a circle centered on the equator at $(J_1, J_2, J_3) = (J, 0, 0)$ with radius $\sim \sqrt{N}/2$ corresponding to the fluctuations of J_2 and J_3 . Points of the circle deviated by ΔJ_3 to the north or south from the equator move in the J_2 direction with velocity $\approx N\chi\Delta J_3$. Thus, Hamiltonian (31) twists the Bloch sphere around axis J_3 . This squeezes the circle into an ellipse, keeping its area constant: thus, noise in some quantum variable decreases while increasing in another. By a suitable rotation of the spin, one can arrange the decreased noise to occur in the variable used for measurements.

As shown in [18], maximum rate at which squeezing is generated by quadratic Hamiltonians is proportional to the difference between the maximum and minimum eigenvalues of the twisting tensor; for OAT with Hamiltonian (31) it is just χ . Note also that for general Hamiltonians a simple formula specifies the maximum rate of squeezing generation in Gaussian states, containing just the second derivatives of the *classical* Hamiltonian [58]. In a geometric interpretation, the squeezing rate can be

related to the difference of principal curvatures of the energy surface.

C. “Spin squeezing” in the classical dynamics

A careful observer could see the OAT effect in the classical motion, as well. Throw up ensemble of plates rotating around axes confined into a narrow circular cone. Let the cone axis be fixed with respect to the plate, lying in the plane of the plate (say, in the direction from the center to the medallion of the Feynman plate). Following the dynamics described in Sec. III A, the rotational axis drifts with respect to the plate with a rate proportional to the rotational axis deviation from the plane of the plate. Consequently, the circular cone of the ensemble changes into an elliptical one. After some time, the directions of the plate rotation become squeezed from one side and stretched perpendicularly.

IV. FREE ASYMMETRIC TOP, TENNIS-RACKET INSTABILITY, AND TWO-AXIS COUNTERTWISTING

Assume a rigid body with the principal moments of inertia $I_1 < I_3 < I_2$, and $K_k = 0$. The equations of motion for the angular velocities are

$$\begin{aligned}\dot{\omega}_1 &= \frac{I_2 - I_3}{I_1} \omega_2 \omega_3, \\ \dot{\omega}_2 &= \frac{I_3 - I_1}{I_2} \omega_3 \omega_1, \\ \dot{\omega}_3 &= \frac{I_1 - I_2}{I_3} \omega_1 \omega_2.\end{aligned}\quad (34)$$

In quantum domain the corresponding Hamiltonian can be cast into the form

$$\hat{H} = \chi_+ \hat{J}_2^2 - \chi_- \hat{J}_1^2 \quad (35)$$

with

$$\begin{aligned}\chi_+ &= \frac{1}{2I_3} - \frac{1}{2I_2} \\ \chi_- &= \frac{1}{2I_1} - \frac{1}{2I_3}.\end{aligned}\quad (36)$$

In the special case of

$$I_3 = \frac{2I_1 I_2}{I_1 + I_2} \quad (37)$$

the Hamiltonian of (35) takes the form

$$\hat{H}_{\text{TACT}} = \chi(\hat{J}_2^2 - \hat{J}_1^2) \quad (38)$$

with

$$\chi = \frac{I_2 - I_1}{4I_1 I_2}. \quad (39)$$

Hamiltonian (38) corresponds to the two-axis counter-twisting (TACT) scenario of spin squeezing [3].

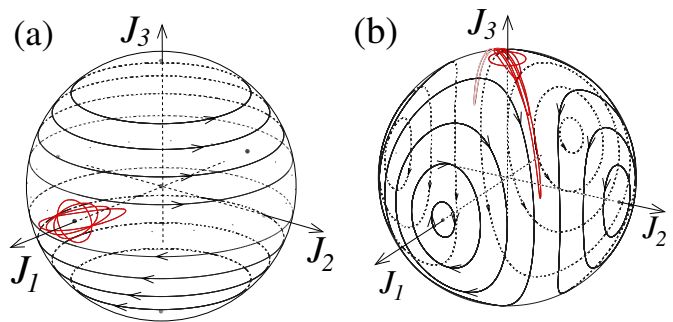


FIG. 3: Evolution of the uncertainty region in spin squeezing scenarios, (a) OAT, (b) TACT.

A. Classical dynamics, Dzhanibekov effect

As is well known from classical mechanics textbooks (see, e.g., [73, 74]), rotations around the two extreme principal axes 1 and 2 are stable, whereas rotation around the intermediate principal axis 3 is unstable. This can be seen by linearizing Eqs. (34) with one of $\omega_{1,2,3}$ much bigger than the remaining two. One can observe this when throwing up a spinning tennis racket: the rotations are stable if the axis of rotation is along the handle (smallest moment of inertia) or perpendicular to the plane of the head of the racket (biggest moment of inertia), and unstable if the axis of rotation is in the plane of the head of the racket, perpendicular to the handle (intermediate moment of inertia). If the initial angular velocity direction is slightly off the stable axis, the rotation axis precesses around it, but if it is slightly off the unstable axis, it diverges away (motion of vector \vec{J} is shown in Fig. 7(a)). The dynamics of the tennis racket was studied in detail in [79–82]. A simple geometric interpretation of stability of the stationary points in terms of the intersecting energy ellipsoid and angular-momentum sphere is discussed in Sec. VIII B.

Typically on Earth, one cannot observe the free spinning body for a long period. However, the effect is spectacular in zero gravity conditions, provided that the initial angular velocity direction is very close to the unstable axis. As the result, one can see the “Dzhanibekov effect” named after Russian cosmonaut Vladimir Dzhanibekov who observed it while in space in 1985: a wing nut rotates while smoothly unscrewing from a screw. When leaving the screw, the nut continues rotating along an axis that is very close to its unstable principal axis. After several turns, the nut suddenly changes its orientation and continues rotating. The orientation switches then continue in regular time intervals. The Dzhanibekov effect was studied in detail in [81–83]. One can understand the motion by realizing that on trajectories that are close to the separatrix, the motion is very slow near the unstable points and relatively fast away from them.

B. Quantum dynamics and spin squeezing

Hamiltonian (38) was first proposed to produce spin squeezing in the TACT scenario in [3]. The mechanism can be visualized on the Bloch sphere as in Fig. 3(b): the sphere is twisted in one sense around J_1 and in the opposite sense around J_2 . Spin states initially polarized along J_3 become squeezed as the uncertainty circle is stretched in one direction and compressed in the other.

The TACT process can generate better squeezing properties than OAT, however, it is much more complicated to be performed with atomic spins than OAT. Therefore, various schemes for achieving effective TACT by applying the OAT twisting Hamiltonian (31) and spin rotations have been proposed [50, 52, 54–56]. Possible physical realizations of TACT were suggested for collective spins based on atomic interactions induced by coherent Raman processes through molecular intermediate states [10, 38], for individual atomic spins by inducing nuclear-electronic spin interaction [43], for Bose-Einstein condensate with spatially modulated nonlinearity [60], for optical fields in resonators with Kerr media [18], nuclear spins via electric quadrupole interaction [64], dipolar spinor condensates [63], or for samples of multilevel atoms interacting with near-resonant cavities [65, 67, 68].

Note that studies of a quantum mechanical asymmetric top go back to the early days of quantum theory [84–91], however, their goal was finding the Hamiltonian spectrum rather than the squeezing dynamics. Even though recently exact diagonalization of the TACT Hamiltonian was studied [59, 70], there was no discussion about the connection to the quantum asymmetric top. We also note that recently an analogy between the tennis racket motion and a driven two-level system was identified, relevant to spin control in nuclear magnetic resonance [92].

V. SYMMETRIC TOP WITH A COAXIAL ROTOR, SPIN TWISTING WITH COAXIAL ROTATION

A. Quantum dynamics

Let us start this section with the quantum case. Using Eq. (27) with $V = 0$ is equivalent to using Hamiltonian (17) in the form

$$\hat{H} = \chi \hat{J}_3^2 + \Omega \hat{J}_3 \quad (40)$$

with $\Omega = \epsilon$ and $\chi = -W$. This corresponds to twisting around axis J_3 and simultaneous rotation around the same axis. Since the Hamiltonian is a function of \hat{J}_3 , its eigenfunctions are those of \hat{J}_3 , i.e., Dicke states with sharp values of J_3 .

The dynamics are split into two possible phases: (a) dominant rotation with $|\chi|N < |\Omega|$, and (b) dominant nonlinearity with $|\chi|N > |\Omega|$. In case (a) the eigenstates corresponding to the extreme eigenvalues of \hat{H} coincide

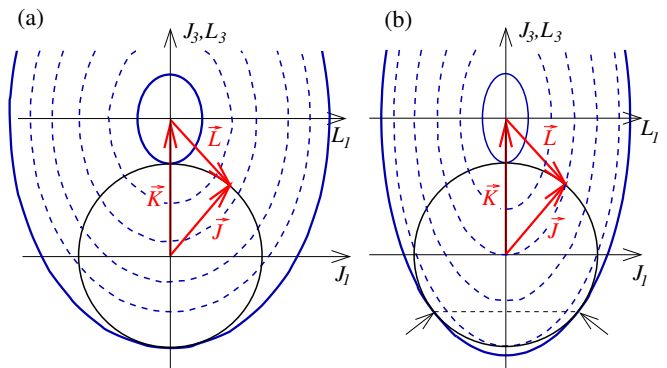


FIG. 4: Constant angular momentum sphere (black) and constant energy ellipsoids (blue) corresponding to a symmetric top with a coaxial rotor. The red vectors \vec{J} and \vec{L} refer to a generic point on the sphere. The maximum and minimum energy ellipsoids compatible with the given value of J are plotted in full line, several other ellipsoids corresponding to intermediate energies are in dashed line. In case (a) the sphere and each of the extreme energy ellipsoids touch at a single point, in case (b) the sphere and the maximum energy ellipsoid touch along a circle (indicated by a dashed line and short arrows).

with the eigenstates corresponding to the extreme eigenvalues of \hat{J}_3 . In case (b) either the ground or the highest excited state of \hat{H} is one of the intermediate eigenstates of \hat{J}_3 . An exception in regime (b) occurs if $\Omega/\chi + N$ is an odd integer; then the ground (or the highest energy) state is degenerate, composed of two nearest Dicke states.

In case (b), the eigenvalue of J_3 corresponding to the extreme energy state is $J_3 = \text{round}[-\Omega/(2\chi)]$ for even N and $J_3 = \text{round}[\frac{1}{2} - \Omega/(2\chi)] - \frac{1}{2}$ for odd N , where $\text{round}[\dots]$ means rounding to the nearest integer. This suggests a way for preparation of arbitrary Dicke states: initialize the system in a spin coherent state which is the ground state of some \hat{J} , and then switch adiabatically the Hamiltonian from $\propto \hat{J}$ to \hat{H} of Eq. (40) with a suitably chosen Ω . If the change is sufficiently slow, the ground state follows the instantaneous Hamiltonian and the system ends up in the chosen Dicke state. The problem is that in the transition from \hat{J} to \hat{H} of (40) some gaps in the energy spectrum close, so that the change would have to be infinitely slow to remain adiabatic. Methods of counterdiabatic driving to overcome this problems have been proposed in [62].

Spin coherent states localized on the Bloch sphere along the parallel $J_3 = -\Omega/(2\chi)$ in case (b) behave similarly as spin coherent states localized along the equator in OAT: the center of the uncertainty area does not move, but the uncertainty circle is deformed into an ellipse and the state become squeezed (squeezing properties of Hamiltonian (40) were studied in [45]).

B. Classical dynamics

The classical model corresponds to a symmetric top, $I_1 = I_2 \neq I_3$, with a coaxial rotor, $K_1 = K_2 = 0 \neq K_3 \equiv K$, such as in Fig. 2(a). The equations of motion and their solution have the same form as those of a free symmetric top, Eqs. (29) and (33), but the precession frequency is changed to

$$\tilde{\Omega} = \frac{(I_3 - I_1)\omega_3 + K}{I_1} = \left(\frac{1}{I_1} - \frac{1}{I_3}\right) J_3 + \frac{K}{I_3}. \quad (41)$$

Similarly to the quantum case, the dynamics are split into two regimes with dominant $|K|/J > |1 - I_3/I_1|$ (a), and $|K|/J < |1 - I_3/I_1|$ (b). The critical parameter is the ratio between the angular momentum K of the rotor and the magnitude of the angular momentum J of the combined system. This can be shown either using the results of the preceding subsection and the correspondence of quantum and classical models, or by the following geometric picture. Consider contact points of the energy ellipsoid and angular momentum sphere as in Fig. 4. In case (a), the lowest energy ellipsoid touches the total angular momentum sphere from outside and the highest energy ellipsoid is touched from inside, both extremal points of contact being on the J_3 axis. In this regime, the only direction of a rotational axis not moving with respect to the body is along J_3 . On the other hand, in case (b) the energy ellipsoid and the total angular momentum sphere touch in a circle that corresponds either to the maximum (plate-like top) or minimum (rod-like top) energy with a given angular momentum. When spun around an axis oriented in that direction, the rotational axis does not move with respect to the body.

As an example, consider a flat symmetric top with $I_1 = I_2 = I_3/2$ as in Fig. 2(a). (The reader can experiment with a simple realization by gluing a fidget-spinner to a light plate.) In this case Eq. (41) yields $\tilde{\Omega} = \omega_3 + 2K/I_3$. Choosing $K = -\frac{1}{2}I_3\omega_3$ leads to $\tilde{\Omega} = 0$, which for $|\omega_{1,2}| \ll |\omega_3|$ means the system is near the boundary between regimes (a) and (b). As a result, a rotational axis close to the symmetry axis of the body keeps its position with respect to the body, and the wobble frequency is equal to the rotation frequency, $\omega_3 + \tilde{\Omega} = \omega_3$.

As another example choose $K = -\frac{3}{4}I_3\omega_3$. This leads to $\tilde{\Omega} = -\omega_3/2$ so that the wobble frequency of a plate is half the rotation frequency, $\omega_3 + \tilde{\Omega} = \omega_3/2$. Thus, with a little cheating of adding a properly spinning rotor, one can force a plate to behave exactly as described in Feynman's cafeteria story [75].

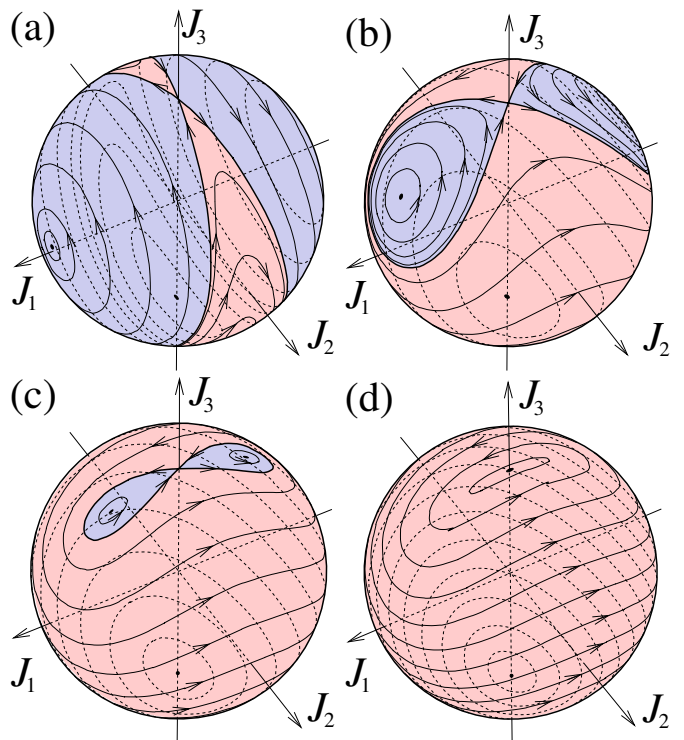


FIG. 5: Angular momentum trajectories for a symmetric top with a perpendicular axis rotor, or a twist-and-turn Hamiltonian (42). The parameters are $\Omega/(\chi J) = 0.2$ (a), 1 (b), 1.7 (c), and 2 (d). Panels (a)-(c) correspond to the Josephson regime with the blue area representing “self-trapped” states. Panel (d) corresponds to the boundary between the Josephson and Rabi regimes where one unstable and two stable stationary points merge, leaving behind one stable stationary point for $\Omega/(\chi J) > 2$.

VI. SYMMETRIC TOP WITH A PERPENDICULAR AXIS ROTOR, TWIST-AND-TURN HAMILTONIAN

A. Quantum dynamics

Let the Hamiltonian have the form

$$\hat{H} = \chi \hat{J}_1^2 + \Omega \hat{J}_3. \quad (42)$$

This is equivalent to the LMG Hamiltonian (27) with $V = W$, $\Omega = \epsilon$ and $\chi = 2V$. The corresponding evolution is twisting around axis J_1 and simultaneous rotation about the perpendicular axis J_3 (also called “twist-and-turn” dynamics [11]).

Assume now for simplicity $N \gg 1$ so that $J \approx N/2$. Similarly as for parallel rotation, there are two distinct regimes: that with dominant rotation $|\Omega| > 2J|\chi|$, and that with dominant twisting $|\Omega| < 2J|\chi|$ (see Fig. 5). This follows from a similar geometric consideration as in the preceding section, or from a general treatment given in Sec. VIII. In the regime of dominant rotation, the Hamiltonian is nondegenerate, with a single maximum

and a single minimum on the Bloch sphere. For $2J\chi = \pm\Omega$ a quantum phase transition occurs with the energy maximum or minimum being split into two, so that in the regime of dominant twisting a saddle point on the Bloch sphere occurs.

The dynamics due to Hamiltonian (42) was studied in [9] as coherent atomic tunneling between two zero-temperature Bose-Einstein condensates confined in a double-well trap, and in [10] as evolution of a two-component condensate. The linear term $\propto \Omega$ corresponds to tunneling of the atoms between the two wells [9] or to Rabi oscillations between the internal states [10], and the nonlinear term $\propto \chi$ refers to the mutual scattering of the atoms. Circling around a single minimum or maximum energy on the Bloch sphere correspond to the oscillation of the condensate between the two wells, whereas trajectories around one of the two local extrema correspond to *self-trapping* of the condensate in one of the wells. Another proposed realization of Hamiltonian (42) is a Bose-Einstein condensate in a ring trap with an optical lattice [57]: two counterpropagating modes are coupled by a periodic potential that changes the propagation direction of the atoms by Bragg reflection (linear term $\propto \Omega$). Sufficiently strong interaction of the atoms (nonlinear term $\propto \chi$) can keep them self-trapped in one of the rotational modes.

In two-state Bose-Einstein condensates, the limiting case of the linear regime with $|\Omega/\chi| \gg N$ has been been dubbed “Rabi regime” whereas the limiting case of the nonlinear regime with $|\Omega/\chi| \ll 1/N$ the “Fock regime”, the transition regime with $1/N \ll |\Omega/\chi| \ll N$ being called “Josephson regime” [93]. As shown in [40], these three regimes correspond to different scaling rules for the dependence of the interferometric phase sensitivity on the atomic number. Experimental observation of transitions between the Josephson and Rabi dynamics in spins of a rubidium Bose-Einstein condensate was reported in [27].

Hamiltonian (42) with suitably chosen ratio of the linear and nonlinear terms has been shown to be especially useful for producing spin squeezed states [11, 18, 58]. Note that the nonlinear term alone as in the OAT scheme tends to align the uncertainty area along the equator (see Fig. 3(a)) so that the squeezing process becomes gradually less efficient. If a linear term with $\Omega = \chi J$ is added, then the uncertainty ellipse is kept inclined by $\pi/4$ from the equator (see the trajectories in Fig. 5(b)) which is the optimum orientation for achieving maximum squeezing rate [18].

B. Classical dynamics

The rigid body dynamics corresponds to a symmetrical top with a perpendicular rotor such as in Fig. 2(b). The “Rabi oscillations” occur in the case with dominant rotor angular momentum, $|K_3|/J > |1 - I_3/I_1|$: the rotational axis of the top circles around the axis of the rotor. If the axis of the body rotation is along the rotor axis, its



FIG. 6: Tennis racket with a rotor along the middle principal axis.

direction is fixed and stable for both co-rotational and counter-rotational orientations.

In the “self trapping” or “Josephson” regime, the angular momentum of the top is dominant, $|K_3|/J < |1 - I_3/I_1|$. In this case, the counter-rotation becomes unstable: the direction opposite to the rotation of the rotor becomes located on a separatrix dividing the 4π sphere of rotational axis orientations into three regions (see Fig. 5 for visualization and Sec. VIII B for more details on stability). In one region the rotational axis circles around the direction of the rotor, in the two other regions the rotational axis circles around a direction pointing between the rotor axis and the symmetry axis of the top. Imagine the Feynman plate supplemented with a perpendicular rotor: if spun around a suitably chosen axis, the rotational axis becomes “self-trapped” with respect to the plate. The plate rotates stably around an axis that is at an angle relative to the plate axis—something that one would never see with common cafeteria plates.

Note that there is no classical analogy of the Fock regime. When translating the condition $|\Omega/\chi| \ll 1/N$ into the Euler-top language with correct dimensionality, one finds $|K_3| \ll \hbar|1 - I_3/I_1|$.

VII. ASYMMETRIC TOP WITH A PRINCIPAL AXIS ROTOR, GENERAL LMG AND QUANTUM PHASE TRANSITIONS

A. Quantum dynamics

Features of the general Hamiltonian (27) have been widely explored, especially with focus on quantum phase transitions and related critical phenomena [21–31]. The concept of quantum phase transition typically refers to closing the gap between the ground and the first excited state by varying a system parameter [6]. In contrast to thermal phase transitions where many states are involved and features of the system are suddenly changed by varying temperature, quantum phase transitions can happen at zero temperature. Rather than thermal, the relevant fluctuations are of quantum nature. Recently the concept has been generalized to excited state quantum phase

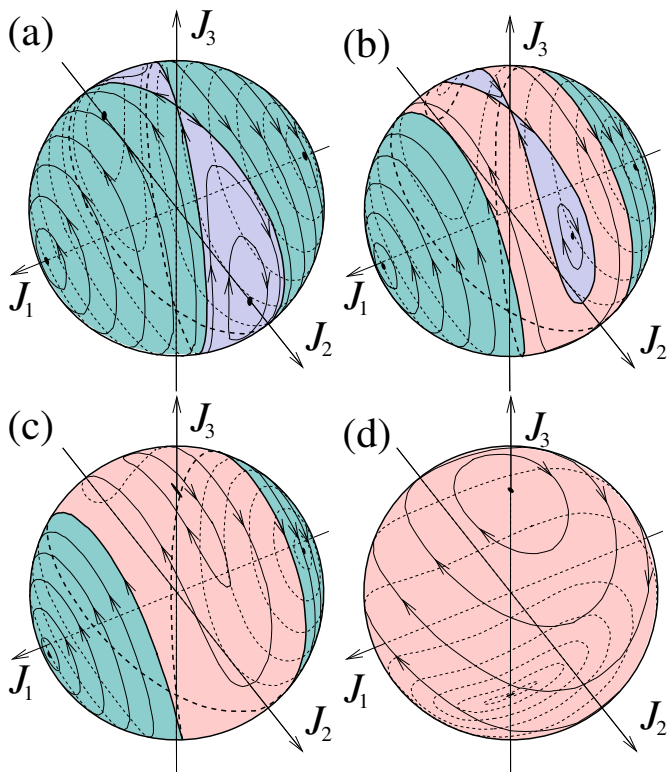


FIG. 7: Angular momentum trajectories for an asymmetric top with a rotor along the middle axis. The twisting parameters of the corresponding quantum Hamiltonian are $\chi_3 = 0$, and $\chi_1 = -10\chi_2$. (a) $\Omega_3 = 0$ (i.e., no rotor), (b) $|\Omega_3| = 1.7J|\chi_2|$, (c) $|\Omega_3| = 2J|\chi_2|$ (critical value for disappearing the saddle point along $+J_3$), and (d) $|\Omega_3| = 2J|\chi_1|$ (critical value for disappearing the saddle point along $-J_3$).

transitions (ESQPT) [7, 8]. In ESQPT, the variation of parameters leads to sudden emergence of singularities in the energy spectrum: in a smooth density of energy levels a peak or a discontinuity occurs. These effects can be related to the Hamiltonian map on the Bloch sphere (see Fig. 7): a discontinuity in the energy spectrum corresponds to a local minimum or maximum of energy on the sphere, and a peak in the energy spectrum corresponds to a saddle point of energy.

B. Classical dynamics

The classical model corresponds to an asymmetric top with a rotor whose axis is aligned with one of the principal axes of the top. Relevant problems include rotational stabilization of rigid bodies [12–14] with applications to attitude control of spacecraft by momentum wheels. Recently, such a model has been used to analyze motion of a diver exerting a twisted somersault [15]: the body of the diver is modeled by an asymmetric top and the moving arms by a rotating disc.

As an example of the ESQPT analogy, let us consider

stabilization of rotation of a tennis racket around the middle principal axis by a rotor as in Fig. 6. The transition is visualized using the Bloch sphere in Fig. 7. With no rotor (Fig. 7(a)), the sphere consists of two pairs of “self-trapped” regions where motion of the angular momenta encircle the stable directions $\pm J_1$ and $\pm J_2$. These regions are separated by a line called separatrix, going through the unstable stationary angular momenta $\pm J_3$.

Adding the rotor with some small angular momentum K_3 , the separatrix splits into two (Fig. 7(b)). A new region between the separatrices emerges as a stripe of trajectories encircling the sphere. With increasing $|K_3|$, the stripe becomes wider and the stable fixed points move towards the unstable points. With a critical value of $|K_3|$, one pair of stable points merge with one unstable point, resulting in a stable point (Fig. 7(c)). This is a new phase in which the racket co-rotating with the rotor around the intermediate principal axis becomes stable, although counter-rotation is still unstable.

With further increasing $|K_3|$, the remaining pair of stable points approach the unstable point till they merge (Fig. 7(d)). For $|K_3|$ above this second critical value the system is in phase with only two stationary angular momenta, both stable.

VIII. STATIONARY ANGULAR MOMENTA AND THEIR STABILITY IN GENERALIZED LMG

Even though the possibility to generalize LMG to arbitrary directions of the linear term was briefly mentioned in [33], we are not aware of any systematic study of such a model. We consider here such a generalization given by Hamiltonian (18) and present a simple geometric approach to find the occurrence of stationary points in the angular momentum space and determine their stability. The results are used to find new cases of ESQPT.

A. Stationary values of the angular momentum

In the angular momentum space, stationary values correspond to the points where the constant energy ellipsoid touches the constant total-angular-momentum sphere. In the classical model, this occurs where the gradient of energy (12) is colinear with the gradient of the squared total momentum (13),

$$\text{grad } E_{\text{body}} = \lambda \text{grad } J^2 \quad (43)$$

for some λ . This leads to the relation between the angular momentum components

$$J_1 = \frac{I_3 K_1 J_3}{(I_3 - I_1) J_3 + I_1 K_3}, \quad (44)$$

$$J_2 = \frac{I_3 K_2 J_3}{(I_3 - I_2) J_3 + I_2 K_3}, \quad (45)$$

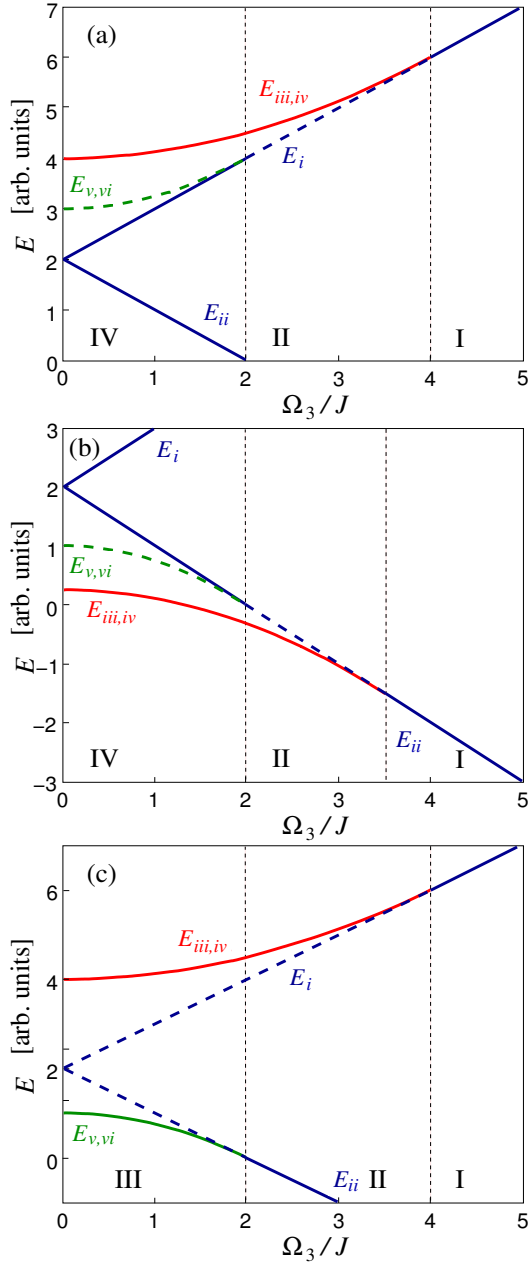


FIG. 8: Energies of the stationary angular momenta, Eqs. (51)—(53), of the original LMG. Full line corresponds to stable, dashed line to unstable values of \vec{J}_{i-vi} . Roman numbers I—IV refer to zones specified in Ref. [24]. The twisting tensor eigenvalues are (in arbitrary units): (a) $\chi_1 = 4$, $\chi_2 = 3$, $\chi_3 = 2$, (b) $\chi_1 = 0.25$, $\chi_2 = 1$, $\chi_3 = 2$, (c) $\chi_1 = 1$, $\chi_2 = 4$, $\chi_3 = 2$.

which, when used in Eq. (13), leads to the polynomial equation for J_3 ,

$$\sum_{n=0}^6 a_n J_3^n = 0, \quad (46)$$

where the coefficients a_n are expressed in Appendix A.

Equation (46) has up to 6 real roots which, together

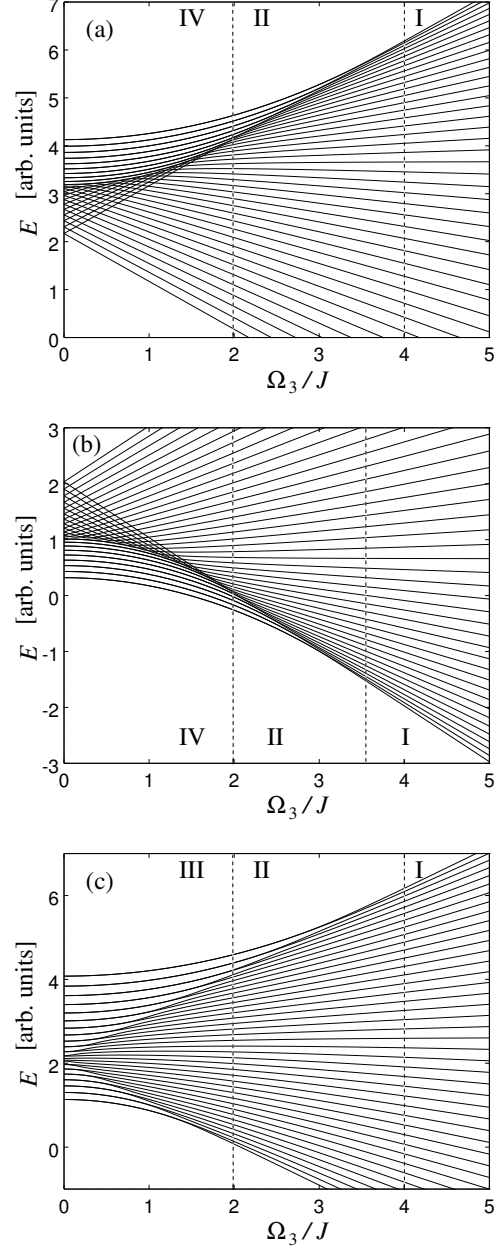


FIG. 9: Eigenvalues of the Hamiltonian (18) with $\Omega_{1,2} = 0$ and the values of $\chi_{1,2,3}$ equal to those of Fig. 8. The number of particles is $N = 40$ (corresponding to $J = 20$ and Hilbert space of 21 states).

with Eqs. (44) and (45), specify the stationary values of \vec{J} .

B. Stationary point stability

There is a simple geometrical picture allowing us to find the stability of a given stationary point. Assume first that the centers of the angular momentum sphere and of the energy ellipsoid are in the same half-space de-

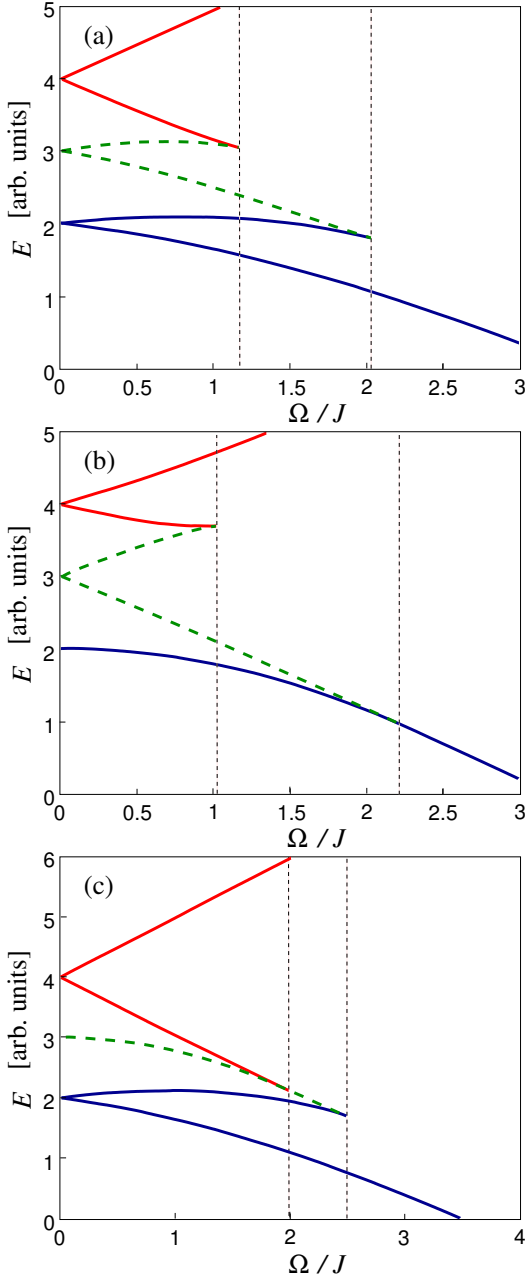


FIG. 10: Energies of the stationary angular momenta of the generalized LMG. Full line corresponds to stable, dashed line to unstable angular momenta. The twisting tensor eigenvalues are (in arbitrary units) $\chi_1 = 4$, $\chi_2 = 3$, $\chi_3 = 2$, the ratio of components of vector $\vec{\Omega}$ are $\Omega_1 : \Omega_2 : \Omega_3$ as follows, (a) 2:1:1, (b) 1:2:0, (c) 2:0:1.

finer by the tangential plane of the contact point. At the point of contact, the energy ellipsoid has two principal radii of curvature, R_1 and R_2 . Assume now that both radii are larger than the radius of the sphere, $R_{1,2} > J$. The ellipsoid then touches the sphere from outside. For slightly higher energy there is no contact between the sphere and the ellipsoid, and for slightly lower energy the ellipsoid and the sphere intersect in a closed curve. Thus,

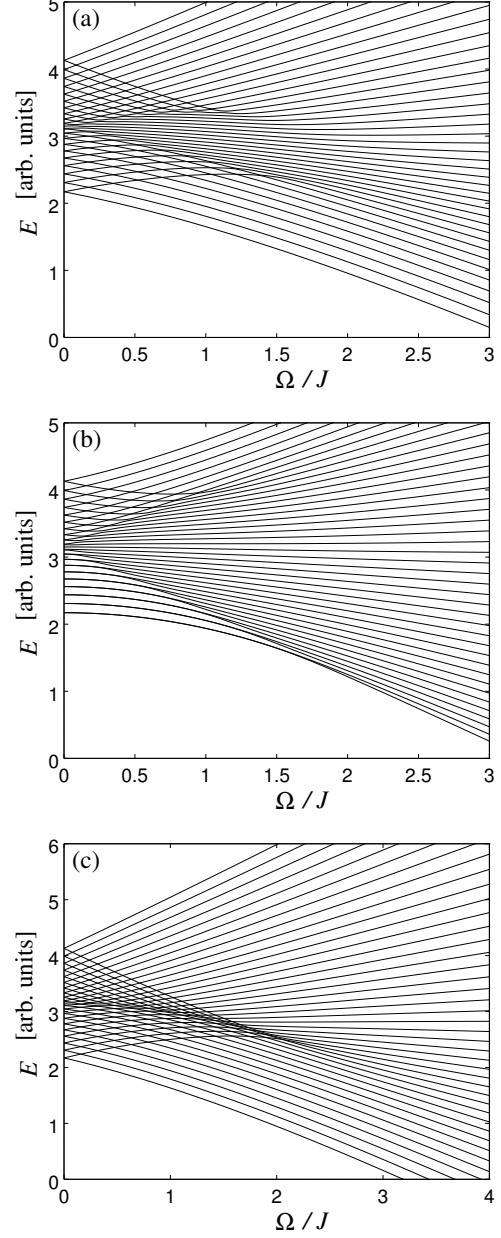


FIG. 11: Eigenvalues of the Hamiltonian (18) of a generalized LMG with the same values of $\chi_{1,2,3}$ and $\Omega_{1,2,3}$ as in Fig. 10. The number of particles is $N = 40$.

the contact point corresponds to a local maximum of energy, i.e., a stable stationary point encircled by states of slightly lower energy. Similarly for both $R_{1,2} < J$ the ellipsoid touches the sphere from inside, and the contact point is stable stationary point of the local energy minimum. On the other hand, if, say, $R_1 < J < R_2$, then there exist two directions along which the ellipsoid radius coincides with J . Along these directions the ellipsoid intersects the sphere. The contact point then corresponds to the energy saddle on the angular momentum sphere, with the intersection lines corresponding to trajectories

approaching to or departing from the (unstable) stationary point.

Assume now that the centers of the sphere and of the ellipsoid are in opposite half-spaces defined by the tangential plane of the contact point. Then the sphere and the ellipsoid touch each other from outside and the contact point corresponds to a stable stationary angular momentum.

In Appendix B we derive the principal curvatures at a general point of an ellipsoid. To analyze various phases then means finding stationary points by solving the algebraic equation (46) and deciding about their stability by finding the principal radii of the energy ellipsoid using Eq. (B25).

C. Special case: phase transitions in the original LMG

Consider first the special situation with $\Omega_1 = \Omega_2 = 0$ (or equivalently $K_1 = K_2 = 0$). To simplify the analysis, assume that $\chi_{1,2,3} > 0$ (one can always achieve this by a suitable additive constant), and suppose that $\chi_{1,2} \neq \chi_3$. In this case Eq. (46) can be factorized as

$$(J_3^2 - J^2) \left[J_3 - \frac{\Omega_3}{2(\chi_1 - \chi_3)} \right]^2 \left[J_3 - \frac{\Omega_3}{2(\chi_2 - \chi_3)} \right]^2 = 0. \quad (47)$$

One can see that the stationary angular momenta are always those with $J_3 = \pm J$ (and thus $J_{1,2} = 0$), and depending on the magnitude of Ω_3 (or K_3), also the vectors with $J_3 = \Omega_3/[2(\chi_{1,2} - \chi_3)]$; the existence of the latter cases depends on whether the resulting J_3 fulfills the condition $|J_3| < J$. Thus, the stationary angular momenta are

$$\vec{J}_{i,ii} = \begin{pmatrix} 0 \\ 0 \\ \pm J \end{pmatrix}, \quad (48)$$

$$\vec{J}_{iii,iv} = \begin{pmatrix} \pm \sqrt{J^2 - \frac{\Omega_3^2}{4(\chi_1 - \chi_3)^2}} \\ 0 \\ \frac{\Omega_3}{2(\chi_1 - \chi_3)} \end{pmatrix}, \quad (49)$$

$$\vec{J}_{v,vi} = \begin{pmatrix} 0 \\ \pm \sqrt{J^2 - \frac{\Omega_3^2}{4(\chi_2 - \chi_3)^2}} \\ \frac{\Omega_3}{2(\chi_2 - \chi_3)} \end{pmatrix}. \quad (50)$$

Stationary vectors $\vec{J}_{i,ii}$ occur always, whereas $\vec{J}_{iii,iv}$ occur when $|\Omega_3| < 2|\chi_1 - \chi_3|J$, and $\vec{J}_{v,vi}$ occur when $|\Omega_3| < 2|\chi_2 - \chi_3|J$.

Energies of the stationary points are obtained from the Hamiltonian, Eq. (18), by substituting values of \vec{J}_{i-vi} for operators \hat{J} . The results can be used as estimates of the

singular points of the energy spectrum. We get

$$E_{i,ii} = \chi_3 J^2 \pm \Omega_3 J, \quad (51)$$

$$E_{iii,iv} = \chi_1 J^2 + \frac{\Omega_3^2}{4(\chi_1 - \chi_3)}, \quad \frac{|\Omega_3|}{J} < 2|\chi_1 - \chi_3| \quad (52)$$

$$E_{v,vi} = \chi_2 J^2 + \frac{\Omega_3^2}{4(\chi_2 - \chi_3)}, \quad \frac{|\Omega_3|}{J} < 2|\chi_2 - \chi_3| \quad (53)$$

To decide about the stability, we find the principal curvature radii of the energy ellipsoid at the stationary points as follows,

$$\vec{J}_i : R_1 = \frac{\chi_3}{\chi_1} \left| J + \frac{\Omega_3}{2\chi_3} \right|, \quad (54)$$

$$R_2 = \frac{\chi_3}{\chi_2} \left| J + \frac{\Omega_3}{2\chi_3} \right|, \quad (55)$$

$$\vec{J}_{ii} : R_1 = \frac{\chi_3}{\chi_1} \left| J - \frac{\Omega_3}{2\chi_3} \right|, \quad (56)$$

$$R_2 = \frac{\chi_3}{\chi_2} \left| J - \frac{\Omega_3}{2\chi_3} \right|, \quad (57)$$

$$\vec{J}_{iii,iv} : R_1 = \frac{\chi_1 J}{\chi_3 \left(1 - \frac{\Omega_3^2}{4\chi_3(\chi_3 - \chi_1)J^2} \right)}, \quad (58)$$

$$R_2 = \frac{\chi_1}{\chi_2}, \quad (59)$$

$$\vec{J}_{v,vi} : R_1 = \frac{\chi_2 J}{\chi_3 \left(1 - \frac{\Omega_3^2}{4\chi_3(\chi_3 - \chi_2)J^2} \right)}, \quad (60)$$

$$R_2 = \frac{\chi_2}{\chi_1}. \quad (61)$$

Comparing the values $R_{1,2}$ with J according to the criteria in Sec. VIII B, we find the following different regimes (see Fig. 8).

1. Case $\chi_3 < \chi_2 < \chi_1$ (Fig. 8(a)): \vec{J}_i is unstable for $2J(\chi_2 - \chi_3) < \Omega_3 < 2J(\chi_1 - \chi_3)$ and stable outside this interval; \vec{J}_{ii} is unstable for $-2J(\chi_1 - \chi_3) < \Omega_3 < -2J(\chi_2 - \chi_3)$ and stable otherwise; $\vec{J}_{iii,iv}$ are stable in the whole interval of their existence $-2J(\chi_1 - \chi_3) < \Omega_3 < 2J(\chi_1 - \chi_3)$ and $\vec{J}_{v,vi}$ are unstable in their whole interval $-2J(\chi_2 - \chi_3) < \Omega_3 < 2J(\chi_2 - \chi_3)$.

Starting from $\Omega_3 = 0$, the system has two degenerate energy minima, two degenerate saddle points, and two degenerate maxima. Varying Ω_3 in the interval $|\Omega_3| < 2J(\chi_2 - \chi_3)$, the degeneracy of the energy minima is lifted, and apart from the degenerate saddles and maxima, the system has one global and one local energy minimum; this corresponds to zone IV defined in [24, 25]. At $|\Omega_3| = 2J(\chi_2 - \chi_3)$ the two saddle points merge with the local energy minimum forming a single saddle point, so that in the intervals $2J(\chi_2 - \chi_3) < |\Omega_3| < 2J(\chi_1 - \chi_3)$ the system has one global energy minimum, one saddle point, and two degenerate energy maxima.

This interval corresponds to zone II of [24]. At $|\Omega_3| = 2J(\chi_3 - \chi_1)$ the two degenerate maxima and the saddle point merge to form a single global maximum. Then, for $2J(\chi_3 - \chi_1) < |\Omega_3|$ the system has just one global energy minimum and one global maximum, corresponding to zone I of [24].

Note that case $\chi_3 < \chi_1 < \chi_2$ has qualitatively the same properties, except that χ_1 and χ_2 change their roles.

2. Case $\chi_1 < \chi_2 < \chi_3$ (Fig. 8(b)): the situation is the same as for $\chi_3 < \chi_2 < \chi_1$, except that the terms $\chi_1 - \chi_3$ and $\chi_2 - \chi_3$ change signs, and maxima and minima switch their roles. Similarly for $\chi_2 < \chi_1 < \chi_3$ where χ_1 and χ_2 change their roles.
3. Case $\chi_1 < \chi_3 < \chi_2$ (Fig. 8(c)): \vec{J}_i is unstable for $-2J(\chi_3 - \chi_1) < \Omega_3 < 2J(\chi_2 - \chi_3)$ and stable outside this interval; \vec{J}_{ii} is unstable for $-2J(\chi_2 - \chi_3) < \Omega_3 < 2J(\chi_3 - \chi_1)$ and stable otherwise. \vec{J}_{iii-vi} are stable in the whole intervals of their existence.

Assume now, to be specific, that $\chi_3 - \chi_1 < \chi_2 - \chi_3$. Starting from $\Omega_3 = 0$ up to $|\Omega_3| = 2J(\chi_3 - \chi_1)$, the degeneracy of the two saddle points is lifted, while there are still two degenerate maxima and two degenerate minima of energy. This regime corresponds to zone III of [24]. At $|\Omega_3| = 2J(\chi_3 - \chi_1)$ the two minima and the lower-energy saddle point merge to form a single global minimum. In the intervals $2J(\chi_3 - \chi_1) < |\Omega_3| < 2J(\chi_2 - \chi_3)$ the system has one global energy minimum, one saddle point and two global energy maxima, corresponding to zone II of [24]. At $|\Omega_3| = 2J(\chi_2 - \chi_3)$ the two maxima and the saddle point merge to form a single energy maximum; for $|\Omega_3| > 2J(\chi_2 - \chi_3)$ the system has one global energy maximum and one minimum, corresponding to zone I of [24].

These results based on a classical analogy can be compared with spectra of quantum Hamiltonians diagonalized numerically. As can be seen comparing Figs. 8 and 9, energies of the stationary points calculated according to Eqs. (51)–(53) clearly match the singularities of the quantum spectra.

D. Phase transitions in the generalized LMG

For general values of $\vec{\Omega}$ one can factorize Eq. (46) numerically. Energies of the resulting values are shown in Fig. 10, and the corresponding Hamiltonian eigenvalues in Fig. 11. The general features are as follows. Starting at $\vec{\Omega} = \vec{0}$, the system has three pairs of degenerate stationary angular momenta with energies $\chi_{1,2,3}J^2$. Ramping up $\vec{\Omega}$, the degeneracy is lifted for those stationary angular momenta in whose direction $\vec{\Omega}$ has a nonzero component. In Figs. 10(a) and 11(a) this is the case for

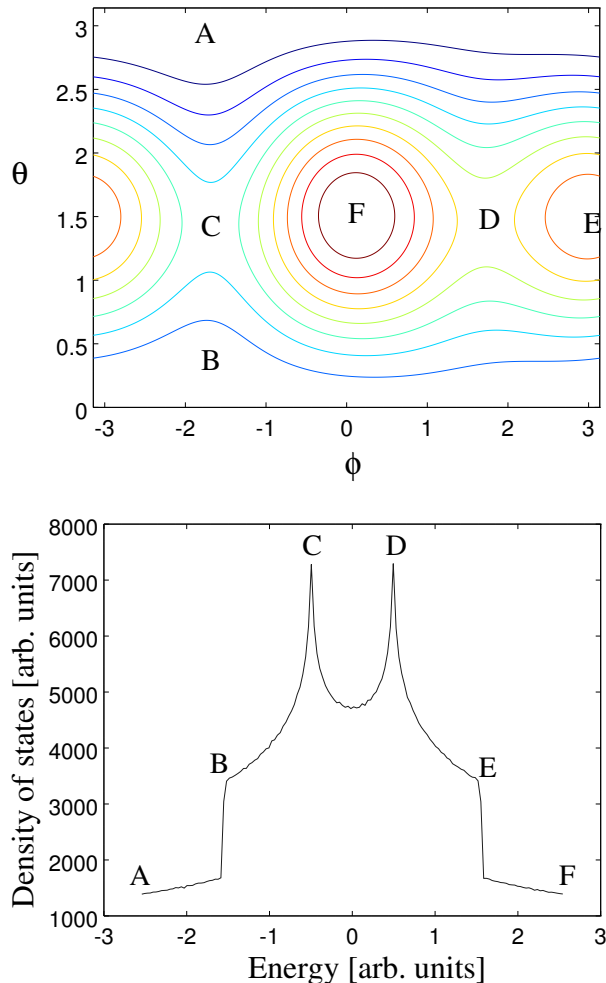


FIG. 12: Upper panel: Contours of the equal energy of the generalized LMG model with $(\chi_1, \chi_2, \chi_3) = (2, 0, -2)$ and $(\Omega_1, \Omega_2, \Omega_3) = (0.5, 0.5, 0.5)$. Coordinates ϕ and θ refer to the direction of vector \vec{J} . Lower panel: energy spectrum corresponding to the same parameters. The beginning and end of the graph correspond to the global minimum and maximum, respectively. The two discontinuities correspond to the local minimum and local maximum, and the peaks correspond to the two saddle points.

all three components (Fig. 12 shows typical energy contours and the corresponding density of states). In Figs. 10(b) and (c) one component of $\vec{\Omega}$ vanishes and the degeneracy of the corresponding energy remains (note that in the original LMG model in Fig. 8 two components vanish so that only one degeneracy is lifted).

One can see that for a general direction, two critical values of Ω occur: at each of them one of the local extrema of energy merges with one of the saddle points and these two stationary points disappear. Thus, it is natural to distinguish three generic phases of the generalized LMG system, according to the number of saddle points of energy on the angular momentum sphere:

those with zero, one, and two saddle points. In case of various symmetries, more detailed classification may be relevant. In particular, considering the original LMG model in [24, 25], two zones were identified within the phase with two saddle points: zone III in which the saddles have different energies, and zone IV with energy degenerate saddles and lifted degeneracy of either energy minima or maxima.

Other special cases can be found in the generalized LMG model if $\vec{\Omega}$ is confined to a plane perpendicular to one of the principal directions of tensor χ . In particular, in the phase with a single saddle point, one of the energy extrema may become degenerate—this is the case of Figs. 10(b) and 11(b) (note that in the original LMG, both energy extrema are degenerate in zone II in which a single saddle occurs). In the phase with two saddle points, one of the energy extrema may become degenerate (Figs. 10(b) and 11(b), or the saddle points can be degenerate (Figs. 10(c) and 11(c)). These cases can be considered as new sub-phases in the generalized LMG model.

IX. FLOQUET TIME CRYSTALS

The concept of time crystals was introduced by F. Wilczek [94, 95], referring to processes in which spontaneous breaking of time symmetry occurs, in analogy to broken spatial symmetry in usual crystals. Interesting phenomena were predicted for systems with periodic driving as so called ‘‘Floquet time crystals’’ [96–98], whose observations have recently been reported in trapped ions [99] and in nitrogen-vacancy centres in diamond [100]. In the Floquet time crystals, the external driving has period τ and thus the Hamiltonian has a discrete time symmetry. Yet, under certain conditions the system behavior breaks this time symmetry and periodic phenomena occur in times corresponding to a multiple of τ , i.e., $n\tau$.

Recently, Floquet time crystal in the LMG model has been proposed [17]. In their scheme, the system is initialized in one of the degenerate energy extremal state. Then, a kick rotates the system around the axis of the LMG linear term by π (in Fig. 7 that would be a π rotation around J_3). As a result, the system swaps to the other degenerate state. If the kicks occur with period τ and the system is initially close to one of the local energy extrema, oscillations of some physical quantity may occur with period 2τ .

It is almost straightforward to build a classical analogue of the LMG Floquet time crystal of [17]. Assume a plate-like symmetric top with $I_2 = I_3 \equiv I_0$, and $I_1 = 2I_0$, with a perpendicular rotor with angular momentum $K_{1,2} = 0$, $K_3 \neq 0$ as in Fig. 13(a). Following Sec. VIII C, two stable stationary angular momenta occur at \vec{J}_{\pm} with $J_1 = \pm\sqrt{J^2 - 4K_3^2}$, $J_2 = 0$, and $J_3 = 2K_3$ for any $J > 2|K_3|$. Assume that the system is prepared near one of these stationary points, say \vec{J}_+ with

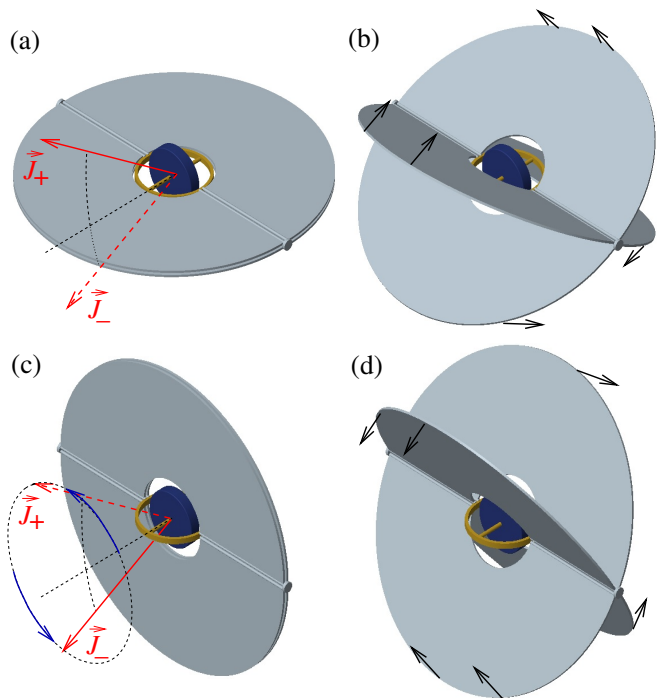


FIG. 13: Reshaping a body in the mechanical analogue of the LMG Floquet time crystal. The body starts as a symmetric top with a perpendicular rotor, having two degenerate stable rotational states with angular momenta \vec{J}_{\pm} (a). The body is then reshaped (b) to take a form of a symmetric top with a coaxial rotor (c) so that the original angular momenta \vec{J}_{\pm} precess around the body axis. After swapping \vec{J}_{\pm} , the body is reshaped (d) back to the original form (a).

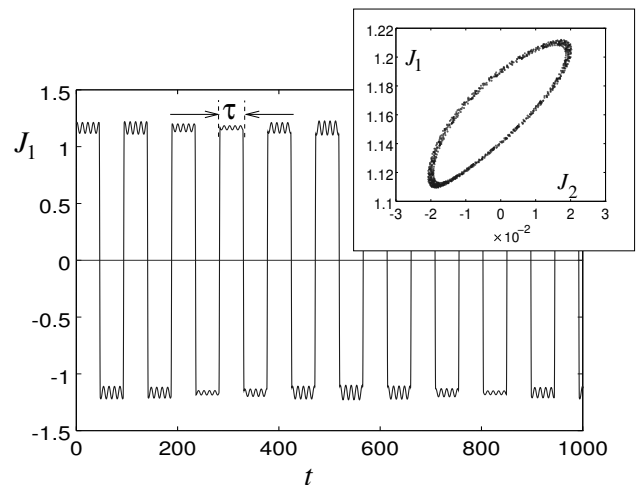


FIG. 14: Evolution of the angular momentum component J_1 in the mechanical Floquet time crystal scenario. The time and angular momentum are dimensionless, their scales following from the choice $I_0 = 1$ and $K_3 = 1$. The initial values are $(J_1, J_2, J_3) = (1.2, 0.02, 1.98)$ and the time parameters are $\tau_0 = 45.20$ and $\tau_{\text{switch}} = 2.09$. Inset: stroboscopic values of $J_{1,2}$ for 1000 repetitions.

$J_1 = +\sqrt{J^2 - 4K_3^2}$. We now need to swap the stationary states. Since a sudden kick instantaneously changing the rotational axis is unphysical, one can consider an alternate scenario. Assume that the body is reshaped, changing the moments of inertia to $I_1 = I_2 = I_0$ and $I_3 = 2I_0$ as in Fig 13(b) and (c), this transformation happening much faster than the precession. After reshaping, the body is a symmetric top with a coaxial rotor. Following Sec. V and Eq. (41), the rotational axis precesses with angular velocity

$$\tilde{\Omega} = \frac{K_3 + J_3}{2I_0}. \quad (62)$$

If $J_3 = 2K_3$, then $\tilde{\Omega} = 3K_3/(2I_0)$ so that after time $\tau_{\text{swap}} = 2\pi I_0/(3K_3)$ the angular momentum is changed to $J_1 = -\sqrt{J^2 - 4K_3^2}$. Then, the body reshapes back (Fig. 13(d)) and continues motion with the rotational axis near the new stationary direction \vec{J}_- . Assume the body is left to evolve, changing periodically its shape from a symmetric top with perpendicular rotor for time τ_0 to a symmetric top with a coaxial rotor for time τ_{swap} . The driving period is $\tau = \tau_0 + \tau_{\text{swap}}$, however, the system returns to the initial stationary angular momentum with period 2τ , as in a Floquet time crystal.

The dynamics is not completely equivalent to the quantum model of [17] where the kick instantaneously rotates each state by the same angle (ideally π). Since $\tilde{\Omega}$ in Eq. (62) depends on J_3 , angular momenta deviating from the stationary values \vec{J}_\pm would, after τ_{swap} , be rotated by different angles. Depending on the system parameters and on the initial state, the deviations may accumulate over time, leading to chaotic dynamics. Nevertheless, one can find intervals of initial values of $J_{1,2,3}$, and of times τ_0 and τ_{swap} , for which regular motion corresponding to a Floquet time crystal is observed. An example of such a motion is in Fig. 14.

X. CONCLUSION

Analogies between the Euler-top dynamics and quantum evolution of collective spins allow us to have simple physical pictures of quantum phenomena such as spin squeezing by OAT or by TACT scenarios. When adding a rotor with axis along one of the principal axes of the top, the system corresponds to the LMG model. We find remarkable the close links between the quantum phase transitions in the LMG model and the behavior of stationary angular momenta in classical rigid body dynam-

ics. Allowing for arbitrary orientation of the rotor axis in the classical domain leads to a generalized LMG model in the quantum domain, predicting new scenarios of quantum phase transitions. These could be observed once a full TACT scheme is implemented (e.g., using the recent proposals [67, 68]) with additional suitable linear terms. Vice versa, the LMG Floquet time crystal proposed in the quantum domain [17] finds its classical counterpart in a periodically reshaped Euler top.

Some questions that remain beyond the present study might be worth further investigation. Is there, within the proposed models, any measurable analogue of the classical body orientation? Taking into account the possibility of multimode spin squeezing [66, 69], is there any relevant scenario of rigid body dynamics to which it would correspond?

Feynman concludes his wobbling-plate story with enthusiasm [75]: *“I went on to work out equations of wobbles. Then I thought about how electron orbits start to move in relativity. Then there’s the Dirac Equation in electrodynamics. And then quantum electrodynamics. [...] It was effortless. It was easy to play with these things. It was like uncorking a bottle: Everything flowed out effortlessly. I almost tried to resist it! There was no importance to what I was doing, but ultimately there was. The diagrams and the whole business that I got the Nobel Prize for came from that piddling around with the wobbling plate.”*

We believe that enthusiasm for physics of wobbling tops is worth sharing. Tossing a coin or throwing up a tennis racket, an attentive observer could see in their motion how spin squeezing works. If some of the readers happen to jump twisted somersaults, they might experience the LMG-type phase transitions themselves. Or, if you are astronaut having some free time on orbit, you might observe self trapping of Bose-Einstein condensates and other critical phenomena in a variant of the Dzhanibekov effect when gluing a fidget spinner to a box you leave rotating.

Acknowledgments

T.O. and L.R. dedicate this paper to J. Tillich who taught us classical mechanics many years ago and raised our interest in the tennis racket instability. T.O. is grateful to P. Cejnar and J. Vidal for stimulating discussions. This work was supported by the Czech Science Foundation, grant No. 17-20479S.

Appendix A: Coefficients of the stationary angular momenta polynomials

Using Eqs. (44) and (45) in Eq. (13) leads to the polynomial equation (46) with coefficients

$$a_0 = -J^2 K_3^4 \frac{I_1^2 I_2^2}{(I_3 - I_1)^2 (I_3 - I_2)^2}, \quad (\text{A1})$$

$$a_1 = -2J^2 K_3^3 \frac{I_1 I_2 (I_1 I_3 - 2I_1 I_2 + I_2 I_3)}{(I_3 - I_1)^2 (I_3 - I_2)^2}, \quad (\text{A2})$$

$$a_2 = \frac{I_1^2 I_2^2 K_3^4 + I_3^2 K_3^2 (I_1^2 K_2^2 + I_2^2 K_1^2) - J^2 K_3^2 [(I_1 I_3 - 2I_1 I_2 + I_2 I_3)^2 + 2I_1 I_2 (I_3 - I_1)(I_3 - I_2)]}{(I_3 - I_1)^2 (I_3 - I_2)^2}, \quad (\text{A3})$$

$$a_3 = \frac{2K_3^3 I_1 I_2 (I_1 I_3 - 2I_1 I_2 + I_2 I_3) + 2K_3 I_3^2 [I_2 (I_3 - I_2) K_1^2 + I_1 (I_3 - I_1) K_2^2]}{(I_3 - I_1)^2 (I_3 - I_2)^2} - \frac{2J^2 K_3 (I_1 I_3 - 2I_1 I_2 + I_2 I_3)}{(I_3 - I_1)(I_3 - I_2)}, \quad (\text{A4})$$

$$a_4 = K_3^2 \frac{(I_1 I_3 - 2I_1 I_2 + I_2 I_3)^2 + 2I_1 I_2 (I_3 - I_1)(I_3 - I_2)}{(I_3 - I_1)^2 (I_3 - I_2)^2} + I_3^2 \left[\frac{K_1^2}{(I_3 - I_1)^2} + \frac{K_2^2}{(I_3 - I_2)^2} \right] - J^2 \quad (\text{A5})$$

$$a_5 = 2K_3 \frac{I_1 I_3 - 2I_1 I_2 + I_2 I_3}{(I_3 - I_1)(I_3 - I_2)}, \quad (\text{A6})$$

$$a_6 = 1. \quad (\text{A7})$$

For the quantum mechanical variables the coefficients are

$$a_0 = -\frac{J^2 \Omega_3^4}{16(\chi_1 - \chi_3)^2 (\chi_2 - \chi_3)^2}, \quad (\text{A8})$$

$$a_1 = \frac{J^2 \Omega_3^3 (\chi_1 + \chi_2 - 2\chi_3)}{4(\chi_1 - \chi_3)^2 (\chi_2 - \chi_3)^2}, \quad (\text{A9})$$

$$a_2 = \Omega_3^2 \frac{\Omega_1^2 + \Omega_2^2 + \Omega_3^2 - 4J^2 [(\chi_1 + \chi_2 - 2\chi_3)^2 + 2(\chi_1 - \chi_3)(\chi_2 - \chi_3)]}{16(\chi_1 - \chi_3)^2 (\chi_2 - \chi_3)^2}, \quad (\text{A10})$$

$$a_3 = \Omega_3 \frac{\Omega_1^2 (\chi_3 - \chi_2) + \Omega_2^2 (\chi_3 - \chi_1) - \Omega_3^2 (\chi_1 + \chi_2 - 2\chi_3)}{4(\chi_1 - \chi_3)^2 (\chi_2 - \chi_3)^2} + J^2 \Omega_3 \frac{\chi_1 + \chi_2 - 2\chi_3}{(\chi_1 - \chi_3)(\chi_2 - \chi_3)}, \quad (\text{A11})$$

$$a_4 = \frac{\Omega_3^2 [(\chi_1 + \chi_2 - 2\chi_3)^2 + 2(\chi_1 - \chi_3)(\chi_2 - \chi_3)]}{4(\chi_1 - \chi_3)^2 (\chi_2 - \chi_3)^2} + \frac{\Omega_1^2}{4(\chi_1 - \chi_3)^2} + \frac{\Omega_2^2}{4(\chi_2 - \chi_3)^2} - J^2, \quad (\text{A12})$$

$$a_5 = -\frac{\Omega_3 (\chi_1 + \chi_2 - 2\chi_3)}{(\chi_1 - \chi_3)(\chi_2 - \chi_3)}, \quad (\text{A13})$$

$$a_6 = 1. \quad (\text{A14})$$

Appendix B: Principal radii of curvature of an ellipsoid

Consider an ellipsoid

$$\left(\frac{x}{a}\right)^2 + \left(\frac{y}{b}\right)^2 + \left(\frac{z}{c}\right)^2 = 1 \quad (\text{B1})$$

which can be parametrized as

$$x = a \sin \theta \cos \phi, \quad (\text{B2})$$

$$y = b \sin \theta \sin \phi, \quad (\text{B3})$$

$$z = c \cos \theta. \quad (\text{B4})$$

In general, one can calculate the principal curvatures $\kappa_{1,2}$ from the mean curvature $H = (\kappa_1 + \kappa_2)/2$ and Gauss curvature $G = \kappa_1 \kappa_2$ as (see, e.g., [102])

$$\kappa_{1,2} = H \pm \sqrt{H^2 - G}, \quad (\text{B5})$$

where

$$H = \frac{g_{11}h_{22} - 2g_{12}h_{12} + g_{22}h_{11}}{2(g_{11}g_{22} - g_{12}^2)}, \quad (\text{B6})$$

$$G = \frac{h_{11}h_{22} - h_{12}^2}{g_{11}g_{22} - g_{12}^2}, \quad (\text{B7})$$

and

$$g_{ij} = \vec{x}_i \cdot \vec{x}_j, \quad (\text{B8})$$

$$\vec{x}_i = \frac{\partial \vec{x}}{\partial u_i}, \quad (\text{B9})$$

$$h_{ij} = \vec{n} \cdot \vec{x}_{ij}, \quad (\text{B10})$$

$$\vec{x}_{ij} = \frac{\partial^2 \vec{x}}{\partial u_i \partial u_j}, \quad (\text{B11})$$

$$\vec{x} = [x, y, z]^T, \quad (\text{B12})$$

and \vec{n} is a unit normal vector to the surface. For the ellipsoid parametrization we use $u_1 = \phi$ and $u_2 = \theta$. We thus find

$$\vec{x}_1 = \begin{pmatrix} -a \sin \theta \sin \phi \\ b \sin \theta \cos \phi \\ 0 \end{pmatrix}, \quad \vec{x}_2 = \begin{pmatrix} a \cos \theta \cos \phi \\ b \cos \theta \sin \phi \\ -c \sin \theta \end{pmatrix}, \quad (\text{B13})$$

so that

$$g_{11} = (a^2 \sin^2 \phi + b^2 \cos^2 \phi) \sin^2 \theta, \quad (\text{B14})$$

$$g_{12} = (b^2 - a^2) \sin \theta \cos \theta \sin \phi \cos \phi, \quad (\text{B15})$$

$$g_{22} = (a^2 \cos^2 \phi + b^2 \sin^2 \phi) \cos^2 \theta + c^2 \sin^2 \theta. \quad (\text{B16})$$

The normal vector is found as

$$\vec{n} = \frac{\vec{x}_1 \times \vec{x}_2}{|\vec{x}_1 \times \vec{x}_2|} = -\frac{1}{Q} \begin{pmatrix} bc \sin^2 \theta \cos \phi \\ ac \sin^2 \theta \sin \phi \\ ab \sin \theta \cos \theta \end{pmatrix}, \quad (\text{B17})$$

where

$$Q = (b^2 c^2 \sin^4 \theta \cos^2 \phi + a^2 c^2 \sin^4 \theta \sin^2 \phi + a^2 b^2 \sin^2 \theta \cos^2 \theta)^{1/2}. \quad (\text{B18})$$

The other important vectors are

$$\vec{x}_{11} = \begin{pmatrix} -a \sin \theta \cos \phi \\ -b \sin \theta \sin \phi \\ 0 \end{pmatrix}, \quad \vec{x}_{12} = \begin{pmatrix} -a \cos \theta \sin \phi \\ b \cos \theta \cos \phi \\ 0 \end{pmatrix}, \quad \vec{x}_{22} = \begin{pmatrix} -a \sin \theta \cos \phi \\ -b \sin \theta \sin \phi \\ -c \cos \theta \end{pmatrix}, \quad (\text{B19})$$

out of which we can calculate

$$h_{11} = \frac{abc \sin^3 \theta}{Q}, \quad (\text{B20})$$

$$h_{12} = 0, \quad (\text{B21})$$

$$h_{22} = \frac{abc \sin \theta}{Q}. \quad (\text{B22})$$

We thus find

$$H = \frac{abc}{2} \cdot \frac{a^2(\sin^2 \phi + \cos^2 \phi \cos^2 \theta) + b^2(\cos^2 \phi + \sin^2 \phi \cos^2 \theta) + c^2 \sin^2 \theta}{(a^2 b^2 \cos^2 \theta + a^2 c^2 \sin^2 \phi \sin^2 \theta + b^2 c^2 \cos^2 \phi \sin^2 \theta)^{3/2}} \quad (\text{B23})$$

and

$$G = \frac{a^2 b^2 c^2}{(a^2 b^2 \cos^2 \theta + a^2 c^2 \sin^2 \phi \sin^2 \theta + b^2 c^2 \cos^2 \phi \sin^2 \theta)^2} \quad (\text{B24})$$

which allow us to find $\kappa_{1,2}$ according to (B5). Expressing then in $\kappa_{1,2}$ angular variables θ, ϕ in terms of the cartesian ones fulfilling Eq. (B1), and taking the reciprocal value of $\kappa_{1,2}$, one finds the principal radii of the ellipsoid in the form

$$R_{1,2} = \frac{2a^2 b^2 c^2 \left(\frac{x^2}{a^4} + \frac{y^2}{b^4} + \frac{z^2}{c^4} \right)^{3/2}}{a^2 + b^2 + c^2 - x^2 - y^2 - z^2 \pm \sqrt{(a^2 + b^2 + c^2 - x^2 - y^2 - z^2)^2 - 4a^2 b^2 c^2 \left(\frac{x^2}{a^4} + \frac{y^2}{b^4} + \frac{z^2}{c^4} \right)}}. \quad (\text{B25})$$

Note that for a sphere $a = b = c = R$ one finds $R_{1,2} = R$. At the vertex of an ellipsoid, $x = a, y = 0, z = 0$, Eq. (B25) yields $R_1 = c^2/a$, and $R_2 = b^2/a$. Along the equator $z = 0$ Eq. (B25) yields

$$R_1 = \frac{1}{ab} \left(\frac{a^2 y^2}{b^2} + \frac{b^2 x^2}{a^2} \right)^{3/2}, \quad R_2 = \frac{c^2}{ab} \left(\frac{a^2 y^2}{b^2} + \frac{b^2 x^2}{a^2} \right)^{1/2}. \quad (\text{B26})$$

-
- [1] R. P. Feynman, R. B. Leighton, and M. Sands, *The Feynman Lectures on Physics*. (Addison Wesley Longman 1970) Volume II Chap. 121.
- [2] L. Euler *Theoria Motus Corporum Solidorum seu Rigidorum*. (A. E. Roser., 1765). Translated in English and annotated by Ian Bruce <http://www.17centurymaths.com/contents/mechanica3.html>.
- [3] M. Kitagawa and M. Ueda, *Squeezed spin states*. Phys. Rev. A **47**, 5138 (1993).
- [4] D. J. Wineland, J. J. Bollinger, W. M. Itano, and D. J. Heinzen, *Squeezed atomic states and projection noise in spectroscopy*. Phys. Rev. A **50**, 67 (1994).
- [5] H. J. Lipkin, N. Meshkov, A.J. Glick, *Validity of many-body approximation methods for a solvable model: (I). Exact solutions and perturbation theory*. Nuclear Physics **62**, 188 (1965).
- [6] S. Sachdev, *Quantum phase transitions*. Physics World **12**, 33 (1999).
- [7] M.A. Caprio, P. Cejnar, and F. Iachello, *Excited state quantum phase transitions in many-body systems*. Annals of Physics **323**, 1106 (2008).
- [8] P. Cejnar, J. Jolie, and R. F. Casten, *Quantum phase transitions in the shapes of atomic nuclei*. Rev. Mod. Phys. **82**, 2155 (2010).
- [9] A. Smerzi, S. Fantoni, S. Giovanazzi, and S. R. Shenoy, *Quantum coherent atomic tunneling between two trapped Bose-Einstein condensates*. Phys. Rev. Lett. **79**, 4950 (1997).
- [10] A. Micheli, D. Jaksch, J. I. Cirac, and P. Zoller, *Many-particle entanglement in two-component Bose-Einstein condensates*. Phys. Rev. A **67**, 013607 (2003).
- [11] W. Muessel, H. Strobel, D. Linnemann, T. Zibold, B. Juliá-Díaz, and M. K. Oberthaler, *Twist-and-turn spin squeezing in Bose-Einstein condensates*. Phys. Rev. A **92**, 023603 (2015).
- [12] P. S. Krishnaprasad and C. A. Berenstein, *On the equilibria of rigid spacecraft with rotors*. Systems & Control Letters **4**, 157-163 (1984).
- [13] A. M. Bloch, P. S. Krishnaprasad, J. E. Marsden, and G. Sánchez de Alvarez, *Stabilization of rigid body dynamics by internal and external torques*. Automatica **28**, 745-756 (1992).
- [14] I. Casu, F. Cret, M. Puta, and A. Voitecovici, *Rigid body with a free spinning rotor and nonlinear stability*. Publicationes Mathematicae - Debrecen **54**, 427-436 (1999).
- [15] S. Bharadwaj, N. Duignan, H. R. Dullin, K. Leung, and W. Tong, *The diver with a rotor*. Indagationes Mathematicae **27**, 11471161 (2016).
- [16] H. R. Dullin and W. Ton, *Twisting Somersault*. SIAM J. Applied Dynamical Systems **15**, 18061822 (2016).
- [17] A. Russomanno, F. Iemini, M. Dalmonte, and R. Fazio, *Floquet time-crystal in the Lipkin-Meshkov-Glick model*. Phys. Rev. B **95**, 214307 (2017).
- [18] T. Opatrný, *Twisting tensor and spin squeezing*. Phys. Rev. A **91**, 053826 (2015).
- [19] R. Montgomery *How much does the rigid body rotate? A Berry's phase from the 18'th century*. Am. J. Phys. **59**, 394 (1991).
- [20] J. Nataro, *An elementary derivation of the Montgomery phase formula for the Euler top*. J. Geom. Mech. **2**, 113 (2010).
- [21] J. Vidal, G. Palacios, and R. Mosseri, *Entanglement in a second-order quantum phase transition*. Phys. Rev. A **69**, 022107 (2004).
- [22] F. Leyvraz and W. D. Heiss, *Large-N Scaling Behavior of the Lipkin-Meshkov-Glick Model*. Phys. Rev. Lett. **95**, 050402 (2005).
- [23] O. Castaños, R. López-Peña, J. G. Hirsch, E. López-Moreno, *Classical and quantum phase transitions in the Lipkin-Meshkov-Glick model*. Phys. Rev. B **74**, 104118 (2006).
- [24] P. Ribeiro, J. Vidal, and R. Mosseri, *Thermodynamical Limit of the Lipkin-Meshkov-Glick Model*. Phys. Rev.

- Let. **99**, 050402 (2007).
- [25] P. Ribeiro, J. Vidal, and R. Mosseri, *Exact spectrum of the Lipkin-Meshkov-Glick model in the thermodynamic limit and finite-size corrections*. Phys. Rev. E **78**, 021106 (2008).
- [26] H. M. Kwok, W. Q. Ning, S. J. Gu, and H. Q. Lin, *Quantum criticality of the Lipkin-Meshkov-Glick model in terms of fidelity susceptibility*. Phys. Rev. E **78**, 032103 (2008).
- [27] T. Zibold, E. Nicklas, C. Gross, and M. K. Oberthaler *Classical Bifurcation at the Transition from Rabi to Josephson Dynamics*. Phys. Rev. Lett. **105**, 204101 (2010).
- [28] C. A. Hooley, P. D. Stevenson, *The Lipkin-Meshkov-Glick model: 'quasi-local' quantum criticality in nuclear physics*. arXiv:1102.1583 (2011).
- [29] G. Engelhardt, V. M. Bastidas, W. Kopylov, and T. Brandes, *Excited-state quantum phase transitions and periodic dynamics*. Phys. Rev. A **91**, 013631 (2015).
- [30] S. Campbell, *Criticality revealed through quench dynamics in the Lipkin-Meshkov-Glick model*. Phys. Rev. B **94**, 184403 (2016).
- [31] A. Gallemí, G. Queraltó, M. Guilleumas, R. Mayol, and A. Sanpera, *Quantum Magnetism with Mesoscopic Bose-Einstein Condensates*. Phys. Rev. A **94**, 063626 (2016).
- [32] S. Dusuel and J. Vidal, *Continuous unitary transformations and finite-size scaling exponents in the Lipkin-Meshkov-Glick model*. Phys. Rev. B **71**, 224420 (2005).
- [33] J. Vidal, *Concurrence in collective models*. Phys. Rev. A **73**, 062318 (2006).
- [34] R. Orus, S. Dusuel, and J. Vidal, *Equivalence of Critical Scaling Laws for Many-Body Entanglement in the Lipkin-Meshkov-Glick Model*. Phys. Rev. Lett. **101**, 025701 (2008).
- [35] J. A. Carrasco, F. Finkel, A. González-López, Miguel A. Rodríguez, and P. Tempesta, *Generalized isotropic LipkinMeshkovGlick models: ground state entanglement and quantum entropies*. J. Stat. Mech.-Theory E. **2016**, 033114 (2016).
- [36] A. Sørensen, L.-M. Duan, J. I. Cirac, and P. Zoller, *Many-particle entanglement with Bose-Einstein condensates*. Nature **409**, 63 (2001).
- [37] C. Orzel, A. K. Tuchman, M. L. Fenselau, M. Yasuda, and M. A. Kasevich, *Squeezed states in a Bose-Einstein condensate*. Science **291**, 2386 (2001).
- [38] K. Helmerson and L. You, *Creating massive entanglement of Bose-Einstein condensed atoms*. Phys. Rev. Lett. **87**, 170402 (2001).
- [39] A. S. Sørensen and K. Mølmer, *Entangling atoms in bad cavities*. Phys. Rev. A **66**, 022314 (2002).
- [40] L. Pezzé, L. A. Collins, A. Smerzi, G. P. Berman, and A. R. Bishop, *Sub-shot-noise phase sensitivity with a Bose-Einstein condensate Mach-Zehnder interferometer*. Phys. Rev. A **72**, 043612 (2005).
- [41] M. Takeuchi, S. Ichihara, T. Takano, M. Kumakura, T. Yabuzaki, and Y. Takahashi, *Spin squeezing via one-axis twisting with coherent light*. Phys. Rev. Lett. **94**, 023003 (2005).
- [42] S. Chaudhury, S. Merkel, T. Herr, A. Silberfarb, I. H. Deutsch, and P. S. Jessen, *Quantum control of the hyperfine spin of a Cs atom ensemble*. Phys. Rev. Lett. **99**, 163002 (2007).
- [43] T. Fernholz, H. Krauter, K. Jensen, J. F. Sherson, A. S. Sørensen, and E. S. Polzik, *Spin squeezing of atomic ensembles via nuclear-electronic spin entanglement*. Phys. Rev. Lett. **101**, 073601 (2008).
- [44] J. Esteve, C. Gross, A. Weller, S. Giovanazzi, and M. K. Oberthaler, *Squeezing and entanglement in a Bose-Einstein condensate*. Nature **455**, 1216 (2008).
- [45] G.-R. Jin, Y.-C. Liu, W.-M. Liu, *Spin squeezing in a generalized one-axis twisting model*. New J. Phys. **11**, 073049 (2009).
- [46] M. H. Schleier-Smith, I. D. Leroux, and V. Vuletić, *Squeezing the collective spin of a dilute atomic ensemble by cavity feedback*. Phys. Rev. A **81**, 021804(R) (2010).
- [47] C. Gross, T. Zibold, E. Nicklas, J. Esteve, and M. K. Oberthaler, *Nonlinear atom interferometer surpasses classical precision limit*. Nature **464**, 1165 (2010).
- [48] M. F. Riedel, P. Böhi, Y. Li, T. W. Hänsch, A. Sinatra, and P. Treutlein, *Atom-chip-based generation of entanglement for quantum metrology*. Nature **464**, 1170 (2010).
- [49] I. D. Leroux, M. H. Schleier-Smith, and V. Vuletić, *Implementation of Cavity Squeezing of a Collective Atomic Spin*. Phys. Rev. Lett. **104**, 073602 (2010).
- [50] Y. C. Liu, Z. F. Xu, G. R. Jin, and L. You, *Spin Squeezing: Transforming One-Axis Twisting into Two-Axis Twisting*. Phys. Rev. Lett. **107**, 013601 (2011).
- [51] M. S. Rudner, L. M. K. Vandersypen, V. Vuletić, and L. S. Levitov, *Generating entanglement and squeezed states of nuclear spins in quantum dots*. Phys. Rev. Lett. **107**, 206806 (2011).
- [52] C. Shen and L. M. Duan, *Efficient spin squeezing with optimized pulse sequences*. Phys. Rev. A **87**, 051801 (2013).
- [53] S. D. Bennett, N. Y. Yao, J. Otterbach, P. Zoller, P. Rabl, and M. D. Lukin, *Phonon-induced spin-spin interactions in diamond nanostructures: application to spin squeezing*. Phys. Rev. Lett. **110**, 156402 (2013).
- [54] J. Y. Zhang, X. F. Zhou, G. C. Guo, and Z. W. Zhou, *Dynamical Spin Squeezing via Higher Order Trotter-Suzuki Approximation*. Phys. Rev. A **90**, 013604 (2014).
- [55] W. Huang, Y.-L. Zhang, C.-L. Zou, X.-B. Zou, and G.-C. Guo, *Two-axis spin squeezing of two-component Bose-Einstein condensates via continuous driving*. Phys. Rev. A **91**, 043642 (2015).
- [56] L.-N. Wu, M. K. Tey, and L. You, *Persistent atomic spin squeezing at the Heisenberg limit*. Phys. Rev. A **92**, 063610 (2015).
- [57] M. Kolář, T. Opatrný, and K. K. Das, *Criticality and spin squeezing in the rotational dynamics of a Bose-Einstein condensate on a ring lattice*. Phys. Rev. A **92**, 043630 (2015).
- [58] T. Opatrný, *Squeezing with classical Hamiltonians*. Phys. Rev. A **92**, 033801 (2015).
- [59] M. Bhattacharya, *Analytical solvability of the two-axis countertwisting spin squeezing Hamiltonian*. arXiv:1509.08530 [quant-ph] (2015).
- [60] T. Opatrný, M. Kolář and K. K. Das, *Spin squeezing by tensor twisting and Lipkin-Meshkov-Glick dynamics in a toroidal Bose-Einstein condensate with spatially modulated nonlinearity*. Phys. Rev. A **91**, 053612 (2015).
- [61] M. Bhattacharya, *Spin squeezing a cold molecule*. Phys. Rev. A **92**, 063823 (2015).
- [62] T. Opatrný, H. Saberi, E. Brion, and K. Mølmer, *Counterdiabatic driving in spin squeezing and Dicke-state preparation*. Phys. Rev. A **93**, 023815 (2016).

- [63] D. Kajtoch and E. Witkowska, *Spin squeezing in dipolar spinor condensates*. Phys. Rev. A **93**, 023627 (2016).
- [64] Y. A. Korkmaz and C. Bulutay, *Nuclear spin squeezing via electric quadrupole interaction*. Phys. Rev. A **93**, 013812 (2016).
- [65] L. Yu, C. Li, J. Fan, G. Chen, T.-C. Zhang, and S. Jia, *Tunable two-axis spin model and spin squeezing in two cavities*. Chin. Phys. B **25**, 050301 (2016).
- [66] I. Kruse, K. Lange, J. Peise, B. Lücke, L. Pezzè, J. Arlt, W. Ertmer, C. Lisdat, L. Santos, A. Smerzi, and C. Klempt, *Improvement of an Atomic Clock using Squeezed Vacuum*. Phys. Rev. Lett. **117**, 143004 (2016).
- [67] Y.-C. Zhang, X.-F. Zhou, X. Zhou, G.-C. Guo, and Z.-W. Zhou, *Cavity-assisted single-mode and two-mode spin-squeezed states via phase-locked atom-photon coupling*. Phys. Rev. Lett. **118**, 083604 (2017).
- [68] J. Borregaard, E. D. Davis, G. S. Bentsen, M. H. Schleier-Smith, and A. S. Sørensen, *One- and two-axis squeezing of atomic ensembles in optical cavities*. arXiv:1706.01650 [quant-ph] (2017).
- [69] T. Opatrný, *Quasicontinuous-variable quantum computation with collective spins in multipath interferometers*. Phys. Rev. Lett. **119**, 010502 (2017).
- [70] F. Pan, Y.-Z. Zhang, and J. P. Draayer *Exact solution of the two-axis countertwisting Hamiltonian*. Annals of Physics **376**, 182 (2017).
- [71] E. M. Chudnovsky and D. A. Garanin, *Spin tunneling via dislocations in Mn-12 acetate crystals*. Phys. Rev. Lett. **87**, 187203 (2001).
- [72] J. Larsen, *Circuit QED scheme for realization of the Lipkin-Meshkov-Glick model*. Europhys. Lett. **90**, 54001 (2010).
- [73] K. R. Symon, *Mechanics* (2nd ed., Addison-Wesley 1960).
- [74] H. Goldstein, *Classical Mechanics* (2nd ed., Addison-Wesley 1980).
- [75] R. P. Feynman, *Surely, You Are Joking, Mr. Feynman!* (Norton, New York, 1985).
- [76] B. Fong Chao, *Feynman's Dining Hall Dynamics*. Physics Today **42**(2), 15 (1989).
- [77] S. Tuleja, B. Gazovic, A. Tomori, and J. Hanc, *Feynman's wobbling plate*. Am. J. Phys. **75**, 240 (2007).
- [78] P. Diaconis, S. Holmes, and R. Montgomery, *Dynamical Bias in the Coin Toss*. SIAM Rev. **49**, 211 (2007).
- [79] M. S. Ashbaugh, C. C. Chicone, and R. H. Cushman, *The Twisting Tennis Racket*. Journal of Dynamics and Differential Equations **3**, 67-85 (1991).
- [80] L. Van Damme, P. Mardešić, and D. Sugny, *The tennis racket effect in a three-dimensional rigid body*. Physica D **338**, 17 (2017).
- [81] H. Murakami, O. Rios, and T. J. Impelluso, *A Theoretical and Numerical Study of the Dzhanibekov and Tennis Racket Phenomena*. J. Appl. Mech. **83**, 111006 (2016).
- [82] O. Rios, T. Ono, H. Murakami, and T. J. Impelluso, *An analytical and geometrical study of the Dzhanibekov and tennis racket phenomena*. Proceedings of the ASME 2016 International Mechanical Engineering Congress and Exposition, IMECE2016 (2016).
- [83] A. G. Petrov and S. E. Volodin, *Janibekovs Effect and the Laws of Mechanics*. Doklady Physics **58**, 349 (2013). Original Russian text published in Doklady Akademii Nauk **451**, 399 (2013).
- [84] E. E. Witmer, *The quantization of the rotational motion of the polyatomic molecule by the new wave mechanics*. Proc. Nat. Acad. Sci. **13**, 60 (1927).
- [85] S. C. Wang, *On the asymmetrical top in quantum mechanics*. Phys. Rev. **34**, 243 (1929).
- [86] G. W. King, R. M. Hainer, and P. C. Cross, *The asymmetric rotor I Calculation and symmetry classification of energy levels*. J. Chem. Phys. **11**, 27 (1943).
- [87] G. W. King, *The Asymmetric Rotor. VI. Calculation of Higher Energy Levels by Means of the Correspondence Principle*. J. Chem. Phys. **15**, 820 (1947).
- [88] C. Van Winter *The asymmetric rotator in quantum mechanics*. Physica **20**, 274 (1954).
- [89] I. Lukac and Ya. A. Smorodinskii, *The wave functions of an asymmetric top*. Soviet Physics JETP **30**, 728 (1970).
- [90] F. Pan and J. P. Draayer, *Algebraic Solutions for the Asymmetric Rotor*. Annals of Physics **275**, 224 (1999).
- [91] V. R. Manfredi and L. Salasnich *Pathological behavior in the spectral statistics of the asymmetric rotor model*. Phys. Rev. E **64**, 066201 (2001).
- [92] L. Van Damme, D. Leiner, P. Mardesic, S. J. Glaser, D. Sugny, *Linking the rotation of a rigid body to the Schrödinger equation: The quantum tennis racket effect and beyond*. Sci. Rep. **7**, 3998 (2017).
- [93] A. J. Leggett, *Bose-Einstein condensation in the alkali gases: Some fundamental concepts*. Rev. Mod. Phys. **73**, 307 (2001).
- [94] F. Wilczek, *Quantum time crystals*. Phys. Rev. Lett. **109**, 160401 (2012).
- [95] A. Shapere and F. Wilczek, *Classical time crystals*. Phys. Rev. Lett. **109**, 160402 (2012).
- [96] K. Sacha, *Modeling spontaneous breaking of time-translation symmetry*. Phys. Rev. A **91**, 033617 (2015).
- [97] D. V. Else, B. Bauer, and C. Nayak, *Floquet time crystals*. Phys. Rev. Lett. **117**, 090402 (2016).
- [98] N. Y. Yao, A. C. Potter, I.-D. Potirniche, and A. Vishwanath, *Discrete time crystals: rigidity, criticality, and realizations*. Phys. Rev. Lett. **118**, 030401 (2017).
- [99] J. Zhang, P. W. Hess, A. Kyprianidis, P. Becker, A. Lee, J. Smith, G. Pagano, I.-D. Potirniche, A. C. Potter, A. Vishwanath, N. Y. Yao, and C. Monroe, *Observation of a discrete time crystal*. Nature **543**, 217 (2017).
- [100] S. Choi, J. Choi, R. Landig, G. Kucsko, H. Zhou, J. Isoya, F. Jelezko, S. Onoda, H. Sumiya, V. Khemani, C. von Keyserlingk, N. Y. Yao, E. Demler, and M. D. Lukin, *Observation of discrete time-crystalline order in a disordered dipolar many-body system*. Nature **543**, 221 (2017).
- [101] K. Sacha and J. Zakrzewski, *Time crystals: a review*. arXiv:1704.03735 (2017).
- [102] M. M. Lipschutz, *Schaum's Outline of Differential Geometry*. (McGraw-Hill, New York, 1969).